10.1117/2.1200912.002501

Bioluminescent imaging and organ-specific metastasis of human cancer cells

Takashi Murakami and Nicole Chun

Applications of high-frequency ultrasound imaging will help reveal the nature of cancer spread.

Cancer metastasis is the end result of a complex series of biological events that lead to the formation of clinically significant secondary tumors at distant sites. Clinical evidence demonstrates that such sites are not randomly located, and certain malignant tumors show a tendency to develop metastases in specific organs (e.g., brain, liver, and lungs).[1] However, an appropriate animal model to characterize the hematogenous nature (i.e., originating in blood) of transplantable human-cancer-cell lines is not available for metastatic cells, while profiling data of hematogenous metastasis has not attracted sufficient scientific attention to improve understanding.

Recent advances in bioluminescent-imaging (BLI)[2] technologies have facilitated quantitative analysis of cellular processes in vivo. BLI reporters have significant signal-to-noise ratios in mammalian tissues, and emitted-light signals can be quantified in intact animals using noninvasive assays. To obtain profiling data of the metastatic fate in human transplantable tumor-cell lines, we have been generating a luciferase-expressing human-cancer-cell library (including melanoma, colon, breast, and prostate cancer) since mid-2007. (Luciferase is an enzyme present in the cells of bioluminescent organisms that produces light by catalyzing the oxidation of luciferin and adenosine triphosphate, ATP, a nucleotide found in the mitochondria of all plant and animal cells.) We created these cells using a retroviral gene-transfer technique. In the presence of D-luciferin, as few as 50 luciferase-transduced cells can be detected in vitro against the background's linear-dose-dependent output of light. Although expression levels among cell lines are not always the same, selected cells provide sufficient numbers of photons in vivo for real-time luminescent imaging.

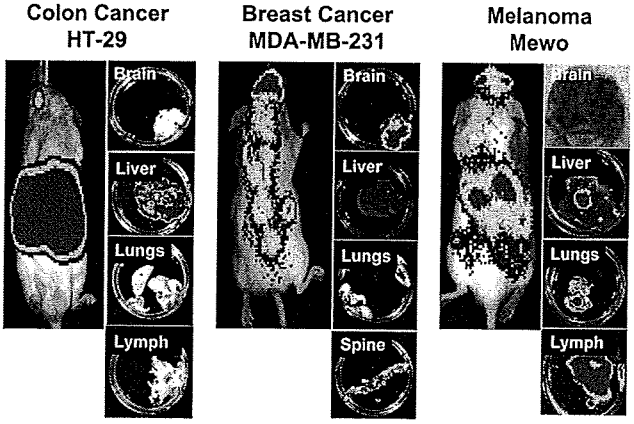

Figure 1. Representative metastatic images of human-cancer-cell lines in nonobese diabetic/severe combined-immunodeficiency mice. Luciferase-expressing cells were injected into the left cardiac ventricle under fine-ultrasonography guidance. In and ex vivo bioluminescence imaging was conducted for (left) HT-29 colon and (middle) MDA-MB-231 breast cancer, and (right) Mewo melanoma cells 30–40 days after tumor implantation. (right) Black dots in the brain represent metastasis of Mewo cells.

To date, cancer-cell injection into mice has been done easily through the tail vein. However, this route is not beneficial for systemic cell delivery because most of the sizable injected cells are trapped in the lung capillaries. To overcome this and systemically deliver cells via arteries, many scientists have blindly tried injections into the left ventricle (heart chamber). Even veteran technicians have blindly been injecting cells into a very narrow space in the mouse heart. However, high-resolution ultrasonography (US), developed specifically for small-animal imaging, now provides clear identification of areas of interest within the myocardial wall (i.e., of the heart muscle) and allows

Continued on next page

precise, site-directed cell injection. Therefore, using fine-US guidance, we have successfully realized accurate and reproducible cardiac-cell injection into mice.

We have generated more than 30 luciferase-expressing human-cancer-cell lines using retroviral transduction. We inoculated these cells into the left cardiac ventricle of nonobese diabetic/severe combined-immunodeficiency (NOD/SCID) mice under fine-US guidance. BLI was conducted for each cell line, and representative organs (e.g., brain, liver, lungs, lymph nodes, bones, and gastrointestinal tract) were then inspected ex vivo. We observed cancer-cell-type-dependent metastasis to specific organs even in mice (beyond the species): see Figure 1. For instance, human colon-cancer HT-29 cells accumulated significantly in the liver of mice, while human-melanoma cell lines showed frequent metastasis to brain, lungs, and lymph nodes in the mouse model. For breast-cancer MDA-MB-231 cells, metastasis was observed to the bone in addition to the brain, lungs, and lymph nodes. Notably, reflecting the clinical features of melanoma, breast, and lung cancer, some cell lines showed preferential metastasis to the brain of mice.

Characteristics common to both tumor cells and normal stem cells appear to exist, referred to as *stemness*. The hallmark traits of stem cells—self-renewal and differentiation capacity—are reflected by the high proliferative capacity and phenotypic plasticity of tumor cells.[3] Since the initial concept of cancer stem cells in solid tumors was established using NOD/SCID mice, we have had to employ animals to apply luciferase-expressing cell behavior to the theory of cancer stem cells. Our recent BLI-based experimentation suggests that a subpopulation of cancer stem cells is essential for organ-selective cancer metastasis.[4]

Approximately 10–20% of all systemic malignancies will eventually metastasize to the brain.[5] Despite this high frequency of brain tumors, an accepted approach for effective treatment is still lacking. Accumulating clinical data suggest that the interaction between chemokines (proteins) and their receptors is a critical component for regulation of tumor progression and metastasis in many cancer types,[1] and that the CXCR4/CXCL12 pathway is involved.[1] However, the pathophysiology in brain metastasis is not fully understood because of the difficulty of creating appropriate animal models. Therefore, BLI combined with high-frequency US imaging should allow various preclinical studies at the tumor/normal-brain interface.

Combining cell resources with an appropriate animal model, our goal for the immediate future, will promote a better and more profound understanding of human-cancer-cell biology. Advances in optical imaging should provide a new platform to accelerate development of therapeutic strategies for human cancer.

This study was supported by a Health and Labor Science Research Grant from the Ministry of Health, Labor, and Welfare (Research on Biological Resources) and the Ministry of Education, Culture, Sports, Science, and Technology (MEXT) of Japan, and a grant from the 'Strategic Research Platform' for Private Universities: Matching Fund Subsidy from MEXT. We thank Masafumi Takahashi for helpful suggestions.

Author Information

Takashi Murakami and Nicole Chun
Jichi Medical University
Simotsuke, Japan

References

1. T. Murakami, A. R. Cardones, and S. T. Hwang, *Chemokine receptors and melanoma metastasis*, **J. Dermatol. Sci. 36**, pp. 71–78, 2004.
2. R. S. Negrin and C. H. Contag, *In vivo imaging using bioluminescence: a tool for probing graft-versus-host disease*, **Nat. Rev. Immunol. 6**, pp. 484–490, 2006.
3. T. Reya, S. J. Morrison, M. F. Clarke, and I. L. Weissman, *Stem cells, cancer, and cancer stem cells*, **Nature 414**, pp. 105–111, 2001.
4. S. Yanagisawa, I. Kadouchi, K. Yokomori, M. Hirose, M. Hakozaki, H. Hojo, K. Maeda, E. Kobayashi, and T. Murakami, *Identification and metastatic potential of tumor-initiating cells in malignant rhabdoid tumor of the kidney*, **Clin. Cancer Res. 5**, pp. 3014–3022, 2009.
5. E. S. Nussbaum, H. R. Djalilian, K. H. Cho, and W. A. Hall, *Brain metastases. Histology, multiplicity, surgery, and survival*, **Cancer 78**, pp. 1781–1788, 1996.

Identification and Metastatic Potential of Tumor-Initiating Cells in Malignant Rhabdoid Tumor of the Kidney

Satohiko Yanagisawa,[1,2] Ichiro Kadouchi,[1] Kinji Yokomori,[2] Masao Hirose,[3] Michiyuki Hakozaki,[4] Hiroshi Hojo,[4] Kosaku Maeda,[2] Eiji Kobayashi,[1] and Takashi Murakami[1]

Abstract **Purpose:** Malignant rhabdoid tumor of the kidney (MRTK) is a rare and highly aggressive malignancy of infanthood. In an effort to delineate MRTK progression, we investigated the metastatic fate of some MRTK cells using xenotransplantation animal models and the tumor-initiating potential of $CD133^+$ MRTK cells.

Experimental Design: We established two MRTK cell lines (JMU-RTK-1 and JMU-RTK-2) from patients with MRTK. We generated five luciferase-expressing MRTK cells for *in vivo* luminescent imaging and evaluated the metastatic fate in an orthotopic xenotransplantation model. Capacities of MRTK-initiating cells were examined in nonobese diabetic/severe combined immunodeficient mice after antibody-mediated magnetic bead sorting. Use of chemokine receptor CXCR4 expression as a metastatic marker was evaluated by flow cytometry and Western blotting.

Results: MRTK cell lines showed distant organ metastasis. JMU-RTK-1, JMU-RTK-2, and G401 cells showed considerable aggressiveness compared with SWT-1 and SWT-2 cells ($P < 0.05$). Moreover, as few as 1,000 $CD133^+$ MRTK cells initiated tumor development in nonobese diabetic/severe combined immunodeficient mice by 21 days (60-100%) in all examined cell lines, although the same number of $CD133^-$ MRTK cells could not form tumors (0%). Interestingly, the metastatic potential of the $CD133^+$ population remained unaffected compared with a nonenriched population. The potential metastatic marker CXCR4 was expressed in $CD133^+$ and $CD133^-$ MRTK cells, and $CD133^-$ cells seemed to play a cooperative role in terms of tumorigenicity and metastasis.

Conclusions: These results suggest that $CD133^+$ cells may determine the metastatic fate of MRTK cells and that $CD133^-$ cells may play an auxiliary role in tumor progression and metastasis.

There seem to be characteristics common to both tumor cells and normal stem cells in terms of what might be referred to as "stemness." The hallmark traits of stem cells—self-renewal and differentiation capacity—are reflected by the high proliferative capacity and phenotypic plasticity of tumor cells (1). Furthermore, malignant tumor cells often lack the terminal differentiation events present in normal cells. These parallels have given rise to the hypothesis that tumors often arise from undifferentiated stem or progenitor cells: Cancer cells can undergo progressive dedifferentiation during their development (1-3). Additionally, it has been proposed that cancer stem cells—a subpopulation of cancer cells possessing tumor-initiating capability—are derived from normal stem cells (1, 4). In fact, since the identification of leukemia-initiating cells, several initiating cells in solid tumors have also been identified for breast (5), brain (6), colon (7, 8), pancreas (9), and prostate cancer (10).

The malignant rhabdoid tumor (MRT) is a rare and highly aggressive malignancy of infanthood, which commonly develops in the kidney and central nervous system (11, 12). Significant progress in genetic studies has revealed that the majority of MRTs harbor biallelic inactivation of the chromatin-remodeling gene *hSNF5/INI1* located in chromosome 22q11.2 (13, 14). However, MRT is resistant to most therapeutic regimens, and the overall survival rate of patients with MRT of the kidney does not exceed 25%. For example, only 8.8% of infants that were diagnosed before the age of 6 months were living 4 years after diagnosis (15). Recent clinical evidence has suggested that a high frequency of tumor-initiating cells in brain tumors (e.g., high-grade medulloblastoma) is significantly correlated with aggressiveness (6).

Authors' Affiliations: [1]Division of Bioimaging Sciences, Center for Molecular Medicine and [2]Department of Pediatric Surgery, Jichi Medical University, Shimotsuke, Tochigi, Japan; [3]Research, Education, and Management Center for Mental and Physical Health, Naruto University of Education, Tokushima, Japan; and [4]First Department of Pathology, Fukushima Medical University School of Medicine, Fukushima, Japan

Received 8/27/08; revised 1/15/09; accepted 1/20/09; published Online First 4/21/09.
Grant support: Health and Labour Science Research Grants from the Ministry of Health, Labor, and Welfare (Research on Biological Resources); the Ministry of Education, Culture, Sports, Science and Technology (MEXT) of Japan (project no. 20591326; 2008); and the "Strategic Research Platform" for Private Universities: matching fund subsidy from MEXT (T. Murakami).
The costs of publication of this article were defrayed in part by the payment of page charges. This article must therefore be hereby marked *advertisement* in accordance with 18 U.S.C. Section 1734 solely to indicate this fact.
Note: Supplementary data for this article are available at Clinical Cancer Research Online (http://clincancerres.aacrjournals.org/).

Requests for reprints: Takashi Murakami, Division of Organ Replacement Research, Center for Molecular Medicine, Jichi Medical University, 3311-1 Yakushiji, Shimotsuke, Tochigi 329-0498, Japan. Phone: 81-285-58-7446; Fax: 81-285-44-5365; E-mail: takmu@jichi.ac.jp

doi:10.1158/1078-0432.CCR-08-2237

Translational Relevance

There is a great deal of clinical evidence supporting the aggressiveness of malignant rhabdoid tumor of the kidney (MRTK). However, an appropriate animal model to characterize the aggressive nature of transplantable MRTK cell lines has not been reported due to the rare malignancy. In this work, we showed the metastatic fate of some MRTK cells using luminescent imaging technology. Moreover, in an effort to understand the aggressiveness of MRTK, we were also able to identify MRTK-initiating (stem) cells from established cell lines. In light of possible distant metastasis in MRTK, we evaluated the relationship between CD133-positive MRTK cells and chemokine receptor CXCR4 expression. These results have yielded important implications concerning MRTK biology, and our transplantable cell source coupled with luminescent imaging provides a tool for new preclinical therapeutic strategies against MRTK.

Moreover, an interesting feature of MRT is the occasional occurrence of separate central nervous system primary tumors (16). Thus, the similarity between high-grade medulloblastoma and MRT in terms of aggressiveness allows us to determine whether MRT cells frequently contain initiating cells.

Herein, we established two MRT cell lines from patients with MRT of the kidney (MRTK) and show that tumor-initiating cells of MRTK are frequently present within the $CD133^+$ population. Furthermore, we show the characteristic metastatic potential of the MRTK cells in an orthotopic xenotransplantation model of severe combined immunodeficient (SCID) mice. Identification and investigation of the characteristics of tumor-initiating cells in MRT can contribute significantly toward the design of aggressive MRT therapies.

Materials and Methods

Cells, animals, and reagents. JMU-RTK-1 and JMU-RTK-2 cell lines were established from two independent patients after confirming the histologic examination using the Japanese Wilms Tumor Study. Histopathologic analysis of the two cases showed that the cells were round to polygonal in shape with vesicular nuclei, prominent nucleoli, and eosinophilic cytoplasm with rare but typical cytoplasmic inclusions. Briefly, the clinical courses of the two patients are described. (*a*) JMU-RTK-1 cells were established from a surgical specimen derived from a 4-mo-old boy who presented with macrohematuria and an abdominal mass (4 cm × 4 cm left kidney mass as determined by abdominal computed tomography). No metastatic lesion was observed at this time. Although the patient received chemotherapy following the surgical treatment, local recurrence and pulmonary metastasis developed and the patient died 5 mo after the recurrence. (*b*) JMU-RTK-2 cells were established from the spinal fluid of 4-mo-old female who primarily presented an abdominal mass (a 6-cm-diameter tumor of the right kidney), although central nervous system metastasis (meningial dissemination) and local recurrence developed following right nephrectomy. The patient died 12 mo after resection of the primary tumor. The Jichi Medical University ethical committee approved of the experiments described in this article.

JMU-RTK-1 and JMU-RTK-2 cells were maintained in DMEM (Sigma-Aldrich) with 10% heat-inactivated FCS and supplements (17). G401 cells (18) were obtained from the Health Science Research Resources Bank (Osaka, Japan) and maintained in McCoy's 5A medium (Life Technologies) with 10% FCS and supplements. SWT-1 and SWT-2 cells (19) were donated by Dr. Masao Hirose (Naruto University of Education, Tokushima, Japan), and FRTK-1 cells (20) were provided by Dr. Michiyuki Hakozaki (Fukushima Medical University, Fukushima, Japan). The well-characterized SWT-1, SWT-2, and FRTK-1 cell lines were used as representative MRTK cells and maintained in RPMI 1640 (Life Technologies) with 10% FCS and supplements. The cultures were kept in a 5% CO_2 and 95% air humidified atmosphere at 37°C.

BALB/c AJcl-nu/nu (BALB/c nude, 6-8 wk old) and C.B-17/Icr-scid/scidJcl (C.B-17 SCID) mice (8-10 wk old) were purchased from CLEA Japan, Inc., and nonobese diabetic (NOD) C.B-17-Prkdc^{scid}/J (NOD/SCID) mice (8-10 wk old) were purchased from Charles River Japan. All experiments in this study were approved by the animal ethics review board of Jichi Medical University and done in accordance with the Jichi Medical University Guide for Laboratory Animals and following the principles of laboratory animal care formulated by the National Society for Medical Research.

Phycoerythrin-conjugated anti-human CD133 (clone AC133; Miltenyi Biotec) and phycoerythrin-conjugated anti-human CXCR4 (clone 12G5; eBioscience) antibodies were used for the flow cytometric analysis. Isotype-matched IgG controls were purchased from BD Pharmingen. For the magnetic separation, anti-phycoerythrin MicroBeads (Miltenyi Biotec) were used for the CD133 cell enrichment.

Establishment of luciferase-expressing MRT cells. Firefly (*Photinus pyralis*) luciferase cDNA from pGL3 basic (Promega) was inserted into the pMSCVpuro retroviral vector (Clontech), generating pMSCV-luciferase (21). GP2-293 packaging cells (Clontech) were cotransfected with pMSCV-luciferase and pVSV-G (Clontech), a plasmid encoding the viral envelope glycoprotein (VSV-G) of vesicular stomatitis virus, using Lipofectamine 2000 (Invitrogen). Supernatants from transfected GP2-293 were incubated with ~50% confluent MRTK cells in the presence of Polybrene (8 mg/mL final concentration; Sigma-Aldrich). Transduced cells were propagated in a medium containing puromycin (Sigma-Aldrich) at 15 mg/mL (luc-JMU-RTK-1, luc-JMU-RTK-2, luc-G401, luc-SWT1, and luc-SWT2).

PCR and reverse transcription-PCR. For reverse transcription-PCR, total RNA was extracted from cells using Isogen (Nippon Gene). Two micrograms of total RNA were used for first-strand synthesis using SuperScript III reverse transcriptase (Invitrogen). The following primers were used for hSNF5/INI1 expression (13): exon 1 sense, 5′-ATGATGATGATGGCGCTGAG-3′; exon 4 sense, 5′-AACCATCAACAG-GAACCGCA-3′; exon 4 antisense, 5′-TGCGGTTCCTGTTGATGGTT-3′; exon 9 antisense, 5′-ATGGAATGTGTACCGGGAAG-3′; glyceraldehyde-3-phosphate dehydrogenase (GAPDH) sense, 5′-GTATCGYGGAAG-GACTCATG-3′; GAPDH antisense, 5′-AGTGGGTGTCGCTGTTGAAG-3′. PCR conditions for each set of primers included initial treatment at 95°C for 2 min, followed by 30 cycles comprising denaturation at 95°C for 15 s, annealing at 57°C for 30 s, and then extension at 72°C for 2 min. PCR products were analyzed by electrophoresis through a 1% agarose gel.

Flow cytometry and magnetic bead selection. Cells (1×10^6) were washed with PBS and incubated with monoclonal antibody (mAb) for 30 min at 4°C. Following washing with 0.1% FCS-PBS, cells were analyzed using FACSCalibur (Becton Dickinson) and FlowJo analysis software (Tree Star). At least 10,000 events were acquired for each sample. For magnetic bead selection, cells (5×10^6) were treated with phycoerythrin-conjugated anti-human CD133 mAb (Miltenyi Biotec), followed by anti-phycoerythrin MicroBeads (Miltenyi Biotec), washed, and then loaded onto a MACS MS column (Miltenyi Biotec) for positive magnet-based selection. The positive and negative fractions were then analyzed by flow cytometry.

Xenogeneic tumor transplantation model. Cells in exponential growth phase were harvested by trypsinization and washed twice in PBS before injection. For the s.c. injections, cells (1×10^3-1×10^5) were

injected into the s.c. space of NOD/SCID mice. To determine the minimal amount of cells capable of engraftment, limiting dilution experiments were done for CD133-positive and CD133-negative cells. Tumor appearance was evaluated using a caliper, and tumor growth at the skin was monitored by calculating the tumor volume (= [length in mm][width in mm]^2/2).

For the orthotopic tumor model of the kidney, C.B-17 SCID mice were treated by injection of anti-asialo GM1 antibodies (100 mg/body, Wako) into the peritoneal cavity 1 d before the operation. The left kidney of anesthetized mice was exposed through a left flank incision and partially exteriorized. Cells (5×10^5) were suspended in 0.1 mL Matrigel (BD Biosciences) and inoculated into the renal subcapsular space. Tumor growth was monitored by *in vivo* luminescent imaging.

Histologic examination. Removed specimens were fixed with 10% paraformaldehyde and embedded in paraffin. Sections were then stained with H&E.

In vivo *and* ex vivo *bioluminescence imaging.* *In vivo* tumor progression was examined using the noninvasive bioimaging system IVIS (Xenogen). Tumor-implanted mice were anesthetized with isoflurane (Abbott Laboratories), and D-luciferin (potassium salt; Biosynth) was injected into the peritoneal cavity at 3 mg/body, which was immediately followed by the measurement of luciferase activity. The imaging system consisted of a cooled, back-thinned charge-coupled device camera to capture both a visible light photograph of the animal taken with light-emitting diodes and the luminescent image. After acquiring photographic images of each mouse, luminescent images were acquired with a 1-min exposure time (21, 22). Images were obtained with a 25-cm field of view, a binning (resolution) factor of 8, 1/f stop, and an open filter. The resulting gray-scale photographic and pseudocolor luminescent images were automatically superimposed using software to facilitate identification of any optical signal and location on the mouse. Optical images were displayed and analyzed using Igor (WaveMetrics) and IVIS Living Image (Xenogen) software packages. The signal from tumors was quantified as photons flux in units of photons/s/cm^2/steradian.

For the inspection of metastasized organs, various organs of mice were resected to examine tumor-derived photons for micrometastases in the presence of D-luciferin. Direct invasion was evaluated for the following representative organs: the gut and omentum, peritoneum, retroperitoneum, diaphragm, spleen, and bladder. For metastasized organs, the lung, liver, brain, and para-aortic lymph nodes of mice were inspected by luminescent imaging (and histologic examination).

Western blot analysis. Cells were lysed using radioimmunoprecipitation assay buffer [50 mmol/L Tris (pH 7.4), 150 mmol/L NaCl, 1% NP40, 0.25% sodium deoxycholate, 1 mmol/L EDTA, 0.1% SDS, 1 mmol/L Na_3VO_4, and 1 mmol/L NaF] containing protease inhibitor cocktail (Roche Diagnostics). Western blot analysis was conducted using standard procedures. SDS-PAGE was done using 1× sample buffer containing 5% β-mercaptoethanol. Following the transfer of proteins to nitrocellulose membranes, the membranes were incubated for 1 h with rabbit anti-human CXCR4 (ProSci) and anti-GAPDH (Santa Cruz Biotechnology) primary antibodies. The membranes were then incubated for 1 h with secondary antibodies. Chemiluminescent detection was done using an ECL Plus Chemiluminescence Detection Kit (GE Healthcare UK Ltd.) and the photo-intensity was quantified by densitometric analysis (NIH image).

Statistical analysis. *P* values based on log-rank, Tukey-Kramer, or Fisher's tests were obtained using Instat (GraphPad) or StatView (Abacus Concepts, Inc.). Differences between groups were considered significant if $P < 0.05$.

Results

Characteristics of established MRTK cell lines. Two cell lines (JMU-RTK-1 and JMU-RTK-2) were established from two patients with MRTK (see Materials and Methods). Both cell lines showed heterogeneous morphology of adherent and spindle cell types on plastic culture dishes. The approximate doubling time in JMU-RTK-1 and JMU-RTK-2 was 9 and 18 h, respectively. Both cell lines were still viable after 200 passages over a 1-year period.

JMU-RTK-1 and JMU-RTK-2 cells were injected s.c. into the flanks of NOD/SCID mice (Fig. 1A). By 21 days, a visible tumor had formed in all mice that underwent the transplantation.

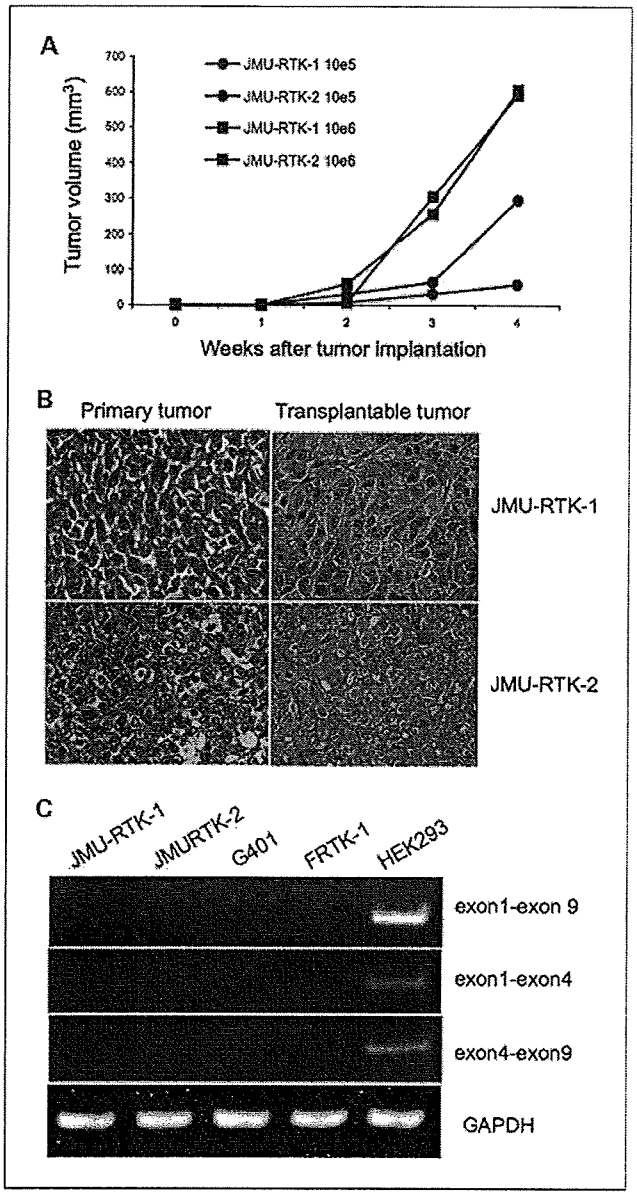

Fig. 1. Characteristics of established MRTK cell lines. *A*, JMU-RTK-1 and JMU-RTK-2 cells (either 1×10^5 or 1×10^6) were transplanted into the subcutaneous space of NOD/SCID mice and tumor growth was measured at the indicated time points. *B*, morphology of established MRTK cell lines following xenogeneic transplantation in nude mice. Left, histology of primary tumors; right, morphology of established cell lines following xenogeneic transplantation in nude mice (at 30 d following tumor implantation; H&E; original magnification, ×200). *C*, analysis of hSNF5/INI1 mRNA expression in established cell lines using reverse transcription-PCR. Top, exon1-exon9; top middle, exon1-exon4; bottom middle, exon4-exon9; bottom, GAPDH as an internal control.

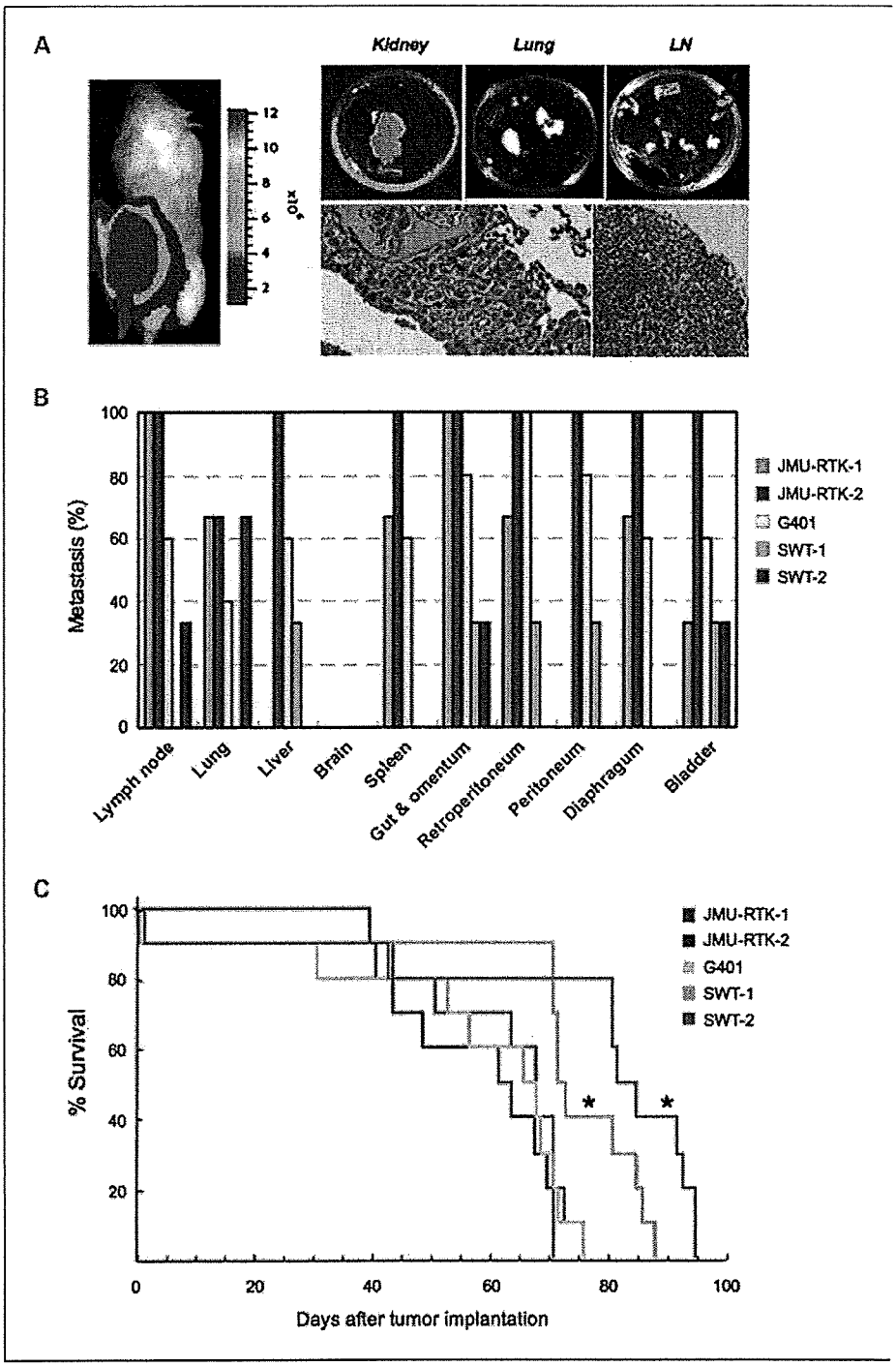

Fig. 2. Metastatic progression of MRTK cell lines in a xenogeneic orthotopic transplantation model. *A*, representative luciferase images of luc-JMU-RTK-1 kidney tumor at day 30 following tumor implantation (*left*). Right top, *ex vivo* inspection of tumor-derived photons; right bottom, microscopic inspection of metastasis in the lungs (*left*; H&E; original magnification, ×100) and the lymph nodes (*LN*; *right*; H&E; original magnification, ×50). *B*, a representative metastatic frequency of luciferase-expressing MRTK cells. Luciferase-expressing MRTK cells were transplanted into the left kidney of SCID mice (3-5 mice per cell line). Tumor-derived photons were examined *ex vivo* 30 d following tumor implantation. One of two independent experiments with similar results. *C*, the survival rate in orthotopically tumor-implanted mice. *, $P < 0.05$ (JMU-RTK-1, JMU-RTK-1, and G401 versus SWT-1 and SWT-2), log-rank test.

Moreover, tumors transplanted into immunodeficient mice showed a similar morphology in comparison with the primary tumor of MRTK (Fig. 1B), and cells in the transplanted tumor were round to polygonal in shape, with vesicular nuclei, prominent nucleoli, and eosinophilic cytoplasm with rare but typical cytoplasmic inclusions.

It is known that loss of function in the *hSNF5/INI1* gene leads to MRT development. In an effort to determine whether the established cell lines were MRT cells, *hSNF5/INI1* expression was examined by reverse transcription-PCR. As shown in Fig. 1C, *hSNF5/INI1 mRNA* transcripts were not detected in the established cell lines. Thus, these results suggest that JMU-RTK-1 and JMU-RTK-2 cells possess a loss of *hSNF5/INI1* gene function.

Metastatic frequency of MRTK cells. Recent advances in luminescent imaging technologies have facilitated the quantitative analysis of cellular processes *in vivo*. JMU-RTK-1 and JMU-RTK-2 cells were transduced with firefly luciferase in an

effort to visualize the fate of tumor progression in the living animals. The advantages associated with the use of luciferase as a marker includes its sensitivity (as few as 100 luciferase-transduced MRTK cells can be detected over the background *in vitro*) and its linear dose-dependent output of light in the presence of D-luciferin (data not shown). Cells (5×10^5 in 0.1 mL Matrigel) were orthotopically implanted into the left renal subcapsular space of C.B-17 SCID mice. Implanted cells rapidly grew at the left kidney, and strong photons were observed around day 7 posttumor implantation. Although the rapid growth in the primary site masked weak photo-signals from potential metastasized sites, metastatic sites at 30 days posttumor implantation were visualized by *ex vivo* inspection in the presence of D-luciferin (Fig. 2A). Invasion to nearby organs was very high in JMU-RTK-1, JMU-RTK-2, and G401 cells. JMU-RTK-1 cells metastasized at the lung and lymph nodes, and JMU-RTK-2 and G401 cells preferentially metastasized in the lung, liver, and lymph nodes. The metastatic frequency and the direct invasion rate to nearby organs were low in SWT-1 and SWT-2 cells (Fig. 2B). These results reflected animal survival following orthotopic tumor injection (Fig. 2C). Thus, these results suggest that JMU-RTK-1, JMU-RTK-2, and G401 cells represent potentially aggressive types in MRTK.

CD133 expression in MRTK cell lines and tumor-initiating capacity in NOD/SCID mice. Recent evidence obtained following the investigation of brain tumors suggests that the frequency of tumor-initiating cells may be significantly correlated with aggressiveness (7). Although the origin in MRT remains unclear, the tumor appears as a result of unique neural differentiation and is distinct from neuroblastoma (23). Thus, the similarity between brain tumors and MRT allows us to determine whether the established cell lines frequently contain MRTK-initiating cells. In an effort to enrich MRTK-initiating cells, the cell surface antigen CD133 was analyzed in MRTK cell lines using a flow cytometer. As shown in Fig. 3, the relative abundance of $CD133^+$ cells was ~4% to 6% in aggressive MRTK cell lines. The $CD133^+$ cells were enriched to 13% to 25% using antibody-mediated magnetic bead sorting. This enrichment of the $CD133^+$

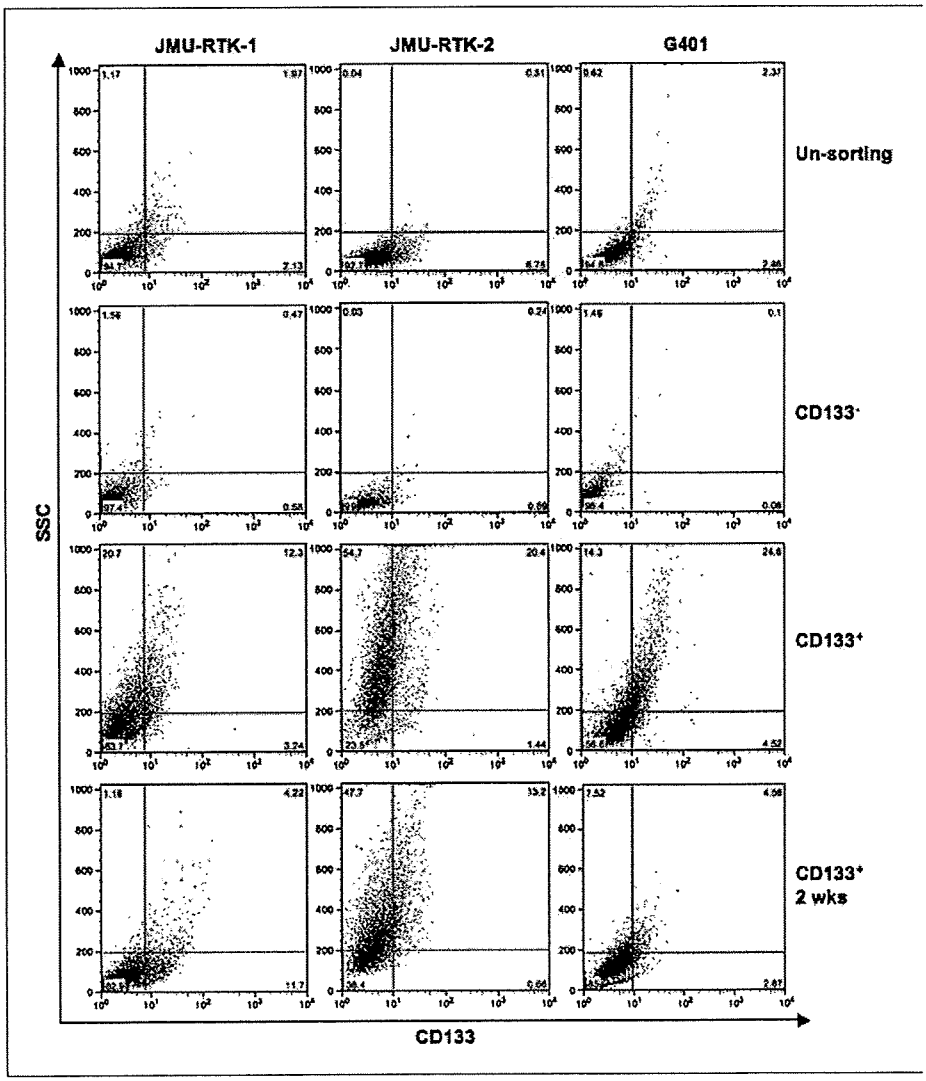

Fig. 3. CD133 expression pattern in MRTK cell lines. Cells were stained with phycoerythrin-conjugated anti-CD133 mAb. Unsorted, unmanipulated cells; $CD133^-$, flow-through fraction following anti-CD133 mAb – mediated magnetic bead selection; $CD133^+$, CD133-enriched fraction following anti-CD133 mAb – mediated magnetic bead selection; CD133 2wks, 2 wk culture population of the CD133-enriched fraction; SSC, side scatter.

population did not always appear to be conserved in the examined cells.

The standard used to evaluate tumor-initiating activity maintains that the candidate cell populations should be able to initiate serially transplantable tumor development. Therefore, we determined and compared the tumor-initiating capacities of $CD133^+$ MRTK cells in NOD/SCID mice (Table 1). As few as 1,000 $CD133^+$ MRTK cells initiated tumor development by 21 days (60-100%), although the same number of $CD133^-$ MRTK cells could not form tumors (0%). Representative serial tumor development in JMU-RTK-1 and JMU-RTK-2 cells is shown in Fig. 4A. Tumor formation was microscopically confirmed in JMU-RTK-1 cells (Fig. 4B). Thus, these results show that MRTK-initiating cells are defined by CD133 expression and that a limited population of $CD133^+$ MRTK-initiating cells can be maintained in culture conditions on plastic dishes. When injected at 1,000 and 10,000 cells, JMU-RTK-1 and JMU-RTK-2 cells formed tumors rapidly (Fig. 4C and D), suggesting that the tumor-initiating potential in JMU-RTK-1 and JMU-RTK-2 cells is higher than that in G401, SWT-1, and SWT-2 cells.

CXCR4 expression in $CD133^+$ MRTK-initiating cells. Our data (see Fig. 2B) suggest that some MRTKs possess marked tendency for distant organ metastasis. Moreover, recent emerging evidence suggests a potential role of the chemokine receptor CXCR4 in tumor-initiating cells and tumor metastasis (9). Therefore, in an effort to determine the correlation between $CD133^+$ MRTK-initiating cells and CXCR4 expression, Western blot analysis using anti-human CXCR4 was done before and after CD133 enrichment in the MRTK cell lines (Fig. 5A). Although unsorted cells expressed CXCR4, some of the cell lines showed increased CXCR4 expression following $CD133^+$ enrichment. Furthermore, fluorescence-activated cell sorting analysis showed cell surface expression of CXCR4 (Fig. 5B), whereas $CD133^-$ cells showed moderate expression of CXCR4.

To determine the metastatic potential in CD133-enriched MRTK cells, orthotopic injection into the left kidney (1,000 cells) was done using $CD133^+$ luciferase-expressing MRTK cells. Although substantial tumor-derived photons were observed at the injection site (data not shown), the resulting metastatic frequency was less correlated with CXCR4 expression levels (Fig. 5C). Thus, some $CD133^+$ MRTK-initiating cells maintained their metastatic potential and the $CD133^-CXCR4^+$ population appeared to play an auxiliary role in tumorigenicity and metastasis.

Table 1. Tumorigenicity of $CD133^+$ MRTK cells in NOD/SCID mice

Cell lines	Cell number	Tumor incidence	
		$CD133^+$	$CD133^-$
JMU-RTK-1	100,000	ND	1/9 (11%)
	10,000	8/9 (89%)*	1/9 (11%)
	1,000	6/9 (67%)*	0/9 (0%)
JMU-RTK-2	100,000	ND	1/6 (17%)
	10,000	4/6 (67%)*	0/6 (0%)
	1,000	4/6 (67%)*	0/6 (0%)
G401	100,000	ND	2/6 (33%)
	10,000	6/6 (100%)*	1/6 (17%)
	1,000	5/6 (80%)*	0/6 (0%)
SWT-1	100,000	ND	1/6 (17%)
	10,000	4/6 (67%)*	0/6 (0%)
	1,000	3/6 (50%)*	0/6 (0%)
SWT-2	100,000	ND	0/6 (0%)
	10,000	4/6 (67%)*	0/6 (0%)
	1,000	4/6 (67%)*	0/6 (0%)
FRTK-1	100,000	ND	3/6 (50%)
	10,000	6/6 (100%)*	1/6 (17%)
	1,000	6/6 (100%)*	0/6 (0%)

NOTE: Cells were injected into the flanks of NOD/SCID mice at the indicated numbers.
Abbreviation: ND, not determined.
*$P < 0.05$ ($CD133^+$ versus $CD133^-$), Fisher's test.

Discussion

We showed that tumorigenic MRTK cells are included in a rare population that expresses CD133. The remarkable features presented in this study include the following: (*a*) the characteristic metastatic fate of MRTK cells in an orthotopic xenotransplantation model of SCID mice; (*b*) $CD133^-$ MRTK cells may play an auxiliary role in tumorigenicity and metastasis.

MRTK cells represent a most progressive rare malignancy of infantile cancers with uncertain histogenesis (11, 12, 15). However, the precise mechanism by which MRTK cells progress is a major interest in cancer biology. Using recent *in vivo* luminescent technology (24, 25), luciferase-labeled MRTK cell lines were used to elucidate the metastatic fate in an orthotopic xenotransplantation model of NOD/SCID mice. Tumor-burdened mice also showed progressiveness in MRTK with distant organ metastasis observed, such as occurred in the liver and lung, in addition to direct invasion of some nearby organs. Thus, these genetically modified transplantable cell lines that were established should provide a useful animal model for the future therapeutic treatment of refractory MRTK.

CD133 was initially described as a surface antigen (a transmembrane pentaspan protein) specific to hematopoietic stem cells (26, 27). Although the biological function of CD133 remains unknown, CD133 is recognized as a stem cell marker for normal and cancerous tissues. In a number of recent studies, monoclonal antibodies against CD133 have been used for the identification and isolation of a putative cancer stem cell population from malignant tumors of brain (6), colon (7, 8), pancreas (9), prostate (10), liver (28, 29), and lung (30). However, our data from the investigation of MRTK cells showed that CD133 expression remains transient and rare even following enrichment using CD133 mAbs. As shown for normal hematopoietic and endothelial progenitors, CD133 expression is limited in early progenitors and usually not detected upon differentiation (26, 27). The present data are consistent with the findings from normal and cancer stem cells as $CD133^+$ subpopulations are exclusively tumorigenic, possess self-renewal capacity, and can differentiate into $CD133^-$ transit-amplifying tumor cells.

Shmelkov et al. (31) also reported that CD133 might not be a suitable marker for colon cancer stem cells. This was elegantly shown using transgenic mice expressing LacZ under control of the CD133 promoter. At least in MRTK, $CD133^+$

cells bore definite tumorigenicity and our data suggest that $CD133^-$ cells may cooperate with $CD133^+$ MRTK cells in terms of tumorigenicity. In human cancers, much evidence has accumulated to provide the consensus that CD133 is a reliable stem cell marker in human cancer specimens. With regard to CD133 expression, it has been shown that seven CD133 mRNA isoforms are controlled by five alternative promoters in a tissue/organ-dependent manner (32). This rather complicated *CD133* gene expression appears to require short-term CD133 expression to retain the organ-specific stem cells. Therefore, further analysis of CD133 transcriptional regulation may provide clues as to how cancer stem cells are regulated between self-renewal and differentiation.

Recent data suggest that the interaction between chemokines and their receptors are also critical components in the regulation of tumor progression and metastasis in many cancer types (33, 34) and that the CXCR4/SDF-1 pathway is involved in the metastatic process of melanoma (17, 34), glioblastoma (35), and colon (36) and pancreatic (37) carcinomas. In fact, clinical studies investigating poor patient prognosis and CXCR4 expression in tumor cells showed a significant correlation for some of the aforementioned malignancies (38–40). Moreover, in the case of pancreatic carcinomas, Hermman et al. (9) showed an important correlation between CXCR4 and CD133 in cancer stem cells, in that a subpopulation of migrating $CXCR4^+CD133^+$ cells is essential for tumor metastasis. Our data (Fig. 5) showed that both $CD133^+$ and $CD133^-$ populations showed CXCR4 expression, thus not entirely consistent with the above report. Our data suggest rather that $CXCR4^+CD133^-$ cells may also contribute to metastatic tumor growth. In this regard, Dalerba and Clarke (41) recently proposed possible models for metastasis-promoting cancer cells, in which $CXCR4^+$ cancer cells act in an auxiliary manner (not unlike the role of macrophages in several tumor model systems; refs. 42, 43). Our data appear to support this proposal. Furthermore, Burns et al. (44) recently reported that an alternate receptor, CXCR7 (RDC1), is expressed in some tumor cells and binds with high affinity to SDF-1. Unlike many other chemokine receptors, ligand activation of CXCR7 does not sufficiently induce migration in tumor cell lines (44) but provides cells with a growth and survival advantage (44–46). Therefore, we speculate that other chemokine receptors may also play a role in the growth and survival advantage of MRTK cells.

Given that MRTK is a progressive malignancy with a poor prognosis and which resists many chemotherapeutic regimens, a new treatment modality to control local disease and prevent systemic progression is required. Recently, it was shown that some MRTK cells express HER-2 and are sensitive to anti-HER-2 humanized mAb upon antibody-dependent cell-mediated cytotoxicity with interleukin 2 (47). Moreover, it has been shown that tumor formation from human melanoma-initiating cells is inhibited by anti-ABC5 mAb through antibody-dependent cell-mediated cytotoxicity (48).

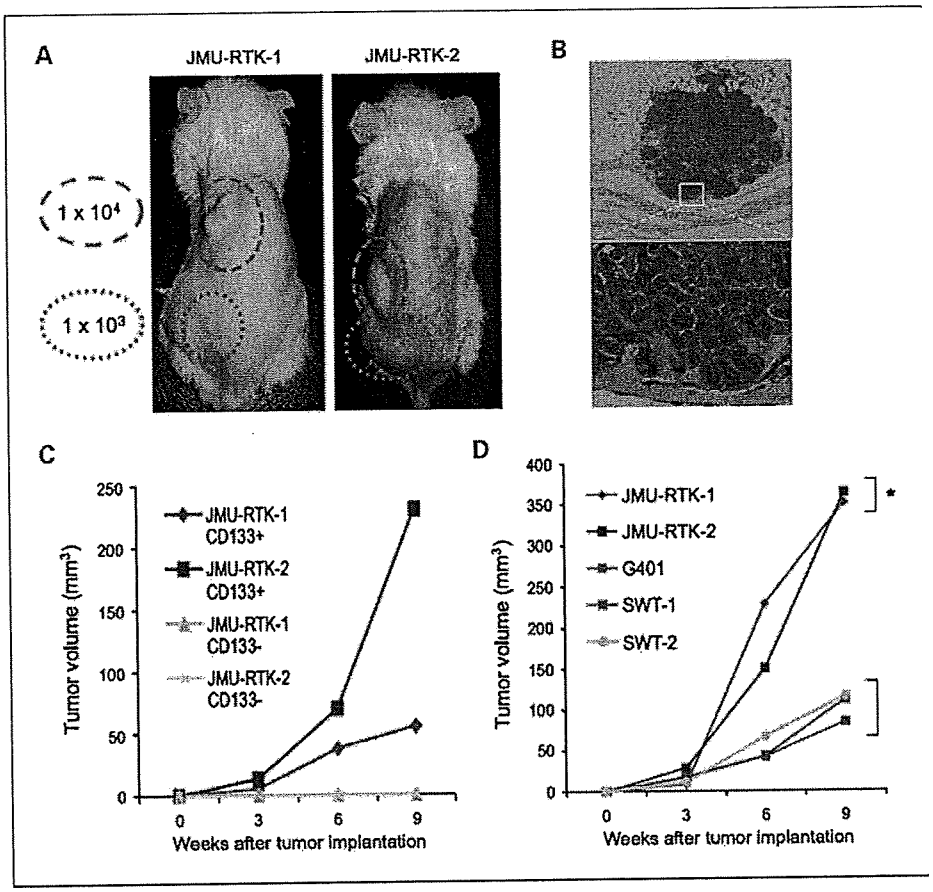

Fig. 4. Tumor growth of $CD133^+$ MRTK enriched cells in NOD/SCID mice. *A*, representative images of JMU-RTK-1 and JMU-RTK-2 tumors at 9 wk following CD133-enriched cell implantation in NOD/SCID mice. CD133-enriched cells (*green dashed*, 1×10^4, and *green dotted*, 1×10^3) were implanted s.c. into the left back of the mice. Notably, CD133-negative cells did not form tumors even with 1×10^5 cells on the right back. *B*, microscopic inspection of CD133-enriched cell implantation (1×10^3 JMU-RTK-1cells). A similar cell morphology is shown in Fig. 1*B*. *C*, JMU-RTK-1 and JMU-RTK-2 cells (1×10^3) following CD133-mediated enrichment were transplanted into the s.c. space of NOD/SCID mice and tumor growth was measured at the indicated time points. *D*, various MRTK cells (1×10^4) following CD133-mediated enrichment in the s.c. space of NOD/SCID mice and tumor growth was measured at the indicated time points. *, $P < 0.05$ (JMU-RTK-1 and JMU-RTK-2, vs G401, SWT-1, and SWT-2), Tukey-Kramer test.

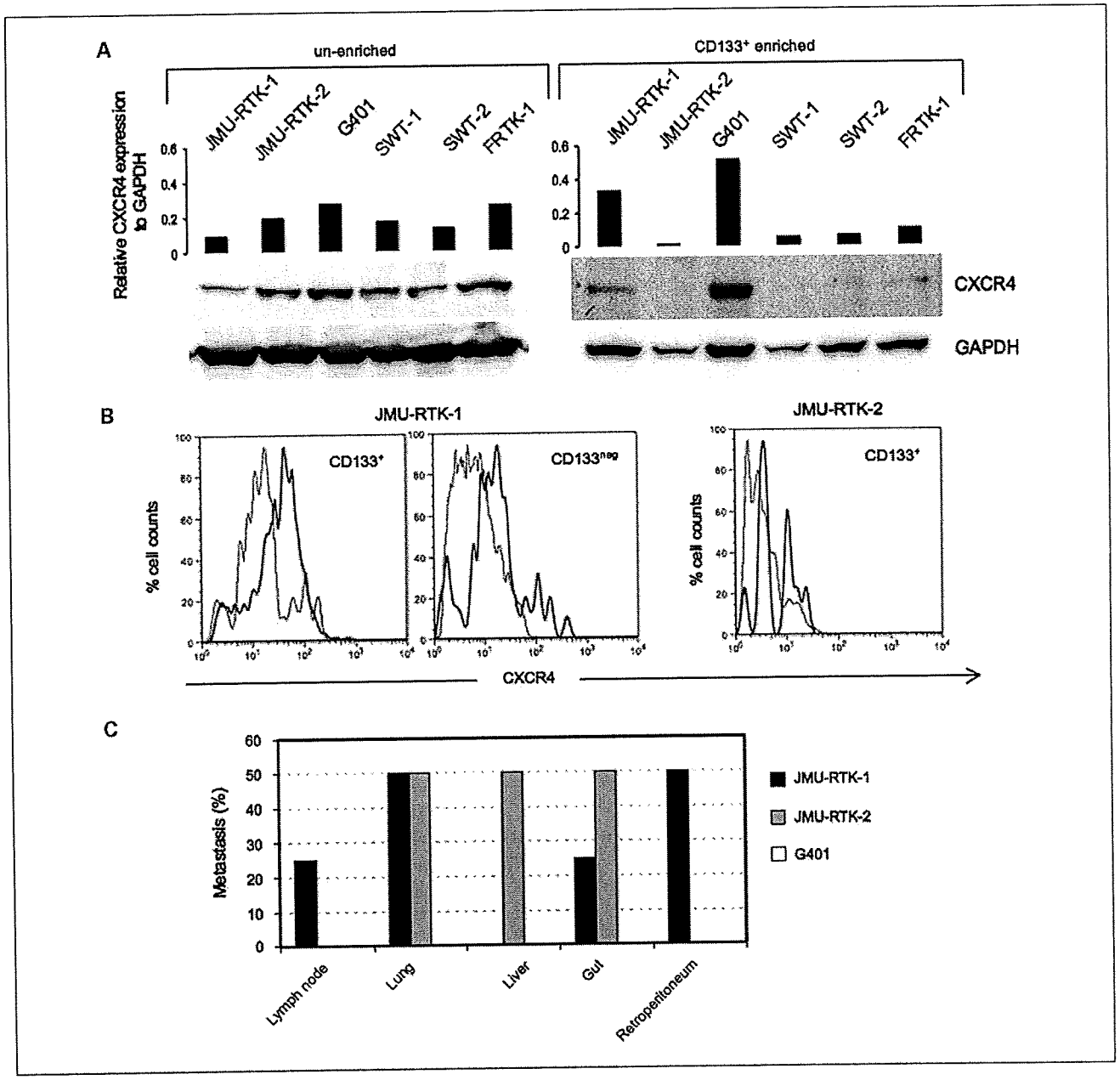

Fig. 5. CXCR4 expression in CD133$^+$-enriched MRTK cells. *A*, Western blot analysis of CXCR4 in MRTK cells. Cells were lysed and analyzed for CXCR4 before and after CD133 enrichment using magnetic bead selection. GAPDH was used as an internal control. One of two independent experiments with similar results. *B*, CXCR4 expression in JMU-RTK-1 and JMU-RTK-2 cells following CD133$^+$ enrichment. CXCR4 expression was analyzed after gating the CD133$^+$ and CD133$^-$ population. Solid line, CXCR4; dashed line, isotype-matched IgG. One of two independent experiments with similar results. *C*, a graph of metastatic frequency of luciferase-expressing MRTK cells following CD133 enrichment. CD133$^+$-enriched cells were transplanted into the left kidney of SCID mice (4-5 mice per cell line). Tumor-derived photons were examined *ex vivo* 30 d following tumor implantation.

Although present therapeutic strategies provide only limited effectiveness against refractory malignancy, the aforementioned evidence suggests that the use of humanized specific antibodies against cancer-initiating cells should provide effective targeting. Although the number of MRTK patients in the present study was very small, our results regarding the identification and characteristics of MRTK-initiating cells provide important implications for the future design of aggressive MRTK therapies.

Disclosure of Potential Conflicts of Interest

No potential conflicts of interest were disclosed.

Acknowledgments

We thank Yasuko Sakuma, Yumi Ohde, and Masayo Kumagai for their skillful technical assistance.

References

1. Reya T, Morrison SJ, Clarke MF, Weissman IL. Stem cells, cancer, and cancer stem cells. Nature 2001;414: 105–11.
2. Beachy PA, Karhadkar SS, Berman DM. Tissue repair and stem cell renewal in carcinogenesis. Nature 2004; 432:324–31.
3. Stingl J, Caldas C. Molecular heterogeneity of breast carcinomas and the cancer stem cell hypothesis. Nat Rev Cancer 2007;7:791–9.
4. Lobo NA, Shimono Y, Qian D, Clarke MF. The biology of cancer stem cells. Annu Rev Cell Dev Biol 2007;23: 675–99.
5. Al-Hajj M, Wicha MS, Benito-Hernandez A, Morrison SJ, Clarke MF. Prospective identification of tumorigenic breast cancer cells. Proc Natl Acad Sci U S A 2003;100:3983–8.
6. Singh SK, Hawkins C, Clarke ID, et al. Identification of human brain tumour initiating cells. Nature 2004;432: 396–401.
7. O'Brien CA, Pollett A, Gallinger S, Dick JE. A human colon cancer cell capable of initiating tumour growth in immunodeficient mice. Nature 2007;445:106–10.
8. Ricci-Vitiani L, Lombardi DG, Pilozzi E, et al. Identification and expansion of human colon-cancer-initiating cells. Nature 2007;445:111–5.
9. Hermann PC, Huber SL, Herrler T, et al. Distinct populations of cancer stem cells determine tumor growth and metastatic activity in human pancreatic cancer. Cell Stem Cell 2007;1:313–23.
10. Collins AT, Berry PA, Hyde C, Stower MJ, Maitland NJ. Prospective identification of tumorigenic prostate cancer stem cells. Cancer Res 2005;65:10946–51.
11. Beckwith J, Palmer N. Histopathology and prognosis of Wilms' tumor: Results of the First National Wilms' Tumor Study. Cancer 1978;41:1937–48.
12. Palmer N, Sutow W. Clinical aspects of the rhabdoid tumor of the kidney. A report of the National Wilms' Tumor Study Group. Med Pediatr Oncol 1983;11:242–5.
13. Versteege I, Sevenet N, Lange J, et al. Truncating mutations of hSNF5/INI1 in aggressive paediatric cancer. Nature 1998;394:203–6.
14. Biegel JA, Zhou JY, Rorke LB, Stenstrom C, Wainwright LM, Fogelgren B. Germ-line and acquired mutations of INI1 in atypical teratoid and rhabdoid tumors. Cancer Res 1999;59:74–9.
15. Tomlinson GE, Breslow NE, Dome J, et al. Rhabdoid tumor of the kidney in the National Wilms' Tumor Study: age at diagnosis as a prognostic factor. J Clin Oncol 2005;23:7641–5.
16. Weeks DA, Beckwith JB, Mierau GW, Luckey DW. Rhabdoid tumor of the kidney. A report of 111 cases from the National Wilms' Tumor Study Pathology Center. Am J Surg Pathol 1989;13:439–58.
17. Murakami T, Maki W, Cardones AR, et al. Expression of CXC chemokine receptor-4 enhances the pulmonary metastatic potential of murine B16 melanoma cells. Cancer Res 2002;62:7328–34.
18. Garvin AJ, Re GG, Tarnowski BI, Hazen-Martin DJ, Sens DA. The G401 cell line, utilized for studies of chromosomal changes in Wilms' tumor, is derived from a rhabdoid tumor of the kidney. Am J Pathol 1993;142: 375–80.
19. Hirose M, Yamada T, Abe T, et al. Establishment and characterization of two cultured cell lines derived from malignant rhabdoid tumors of the kidney. Int J Cancer 1996;67:218–23.
20. Hakozaki M, Hojo H, Sato M, et al. Establishment and characterization of a new cell line, FRTK-1, derived from human malignant rhabdoid tumor of the kidney, with overexpression of epidermal growth factor receptor and cyclooxygenase-2. Oncol Rep 2006;16: 265–71.
21. Sato A, Ohtsuki M, Hata M, Kobayashi E, Murakami T. Antitumor activity of IFN-λ in murine tumor models. J Immunol 2006;176:7686–94.
22. Murakami T, Sato A, Chun NA, et al. Transcriptional modulation using HDACi depsipeptide promotes immune cell-mediated tumor destruction of murine B16 melanoma. J Invest Dermatol 2008; 128:1506–16.
23. Higashino K, Narita T, Taga T, Ohta S, Takeuchi Y. Malignant rhabdoid tumor shows a unique neural differentiation as distinct from neuroblastoma. Cancer Sci 2003;94:37–42.
24. Contag CH, Bachmann MH. Advances in *in vivo* bioluminescence imaging of gene expression. Annu Rev Biomed Eng 2002;4:235–60.
25. Weissleder R, Pittet MJ. Imaging in the era of molecular oncology. Nature 2008;452:580–9.
26. Miraglia S, Godfrey W, Yin AH, et al. A novel five-transmembrane hematopoietic stem cell antigen: isolation, characterization, and molecular cloning. Blood 1997;90:5013–21.
27. Yin AH, Miraglia S, Zanjani ED, et al. AC133, a novel marker for human hematopoietic stem and progenitor cells. Blood 1997;90:5002–12.
28. Suetsugu A, Nagaki M, Aoki H, et al. Characterization of CD133$^+$ hepatocellular carcinoma cells as cancer stem/progenitor cells. Biochem Biophys Res Commun 2006;351:820–4.
29. Yin S, Li J, Hu C, et al. CD133 positive hepatocellular carcinoma cells possess high capacity for tumorigenicity. Int J Cancer 2007;120:1444–50.
30. Eramo A, Lotti F, Sette G, et al. Identification and expansion of the tumorigenic lung cancer stem cell population. Cell Death Differ 2008;15:504–14.
31. Shmelkov SV, Butler JM, Hooper AT, et al. CD133 expression is not restricted to stem cells, and both CD133$^+$ and CD133$^-$ metastatic colon cancer cells initiate tumors. J Clin Invest 2008;118:2111–20.
32. Shmelkov SV, Jun L, St Clair R, et al. Alternative promoters regulate transcription of the gene that encodes stem cell surface protein AC133. Blood 2004; 103:2055–61.
33. Balkwill F. Cancer and the chemokine network. Nat Rev Cancer 2004;4:540–50.
34. Murakami T, Cardones AR, Hwang ST. Chemokine receptor and melanoma metastasis. J Dermatol Sci 2004;36:71–8.
35. Rubin JB, Kung AL, Klein RS, et al. A small-molecule antagonist of CXCR4 inhibits intracranial growth of primary brain tumors. Proc Natl Acad Sci U S A 2003;100:13513–8.
36. Zeelenberg IS, Ruuls-Van Stalle L, Roos E. The chemokine receptor CXCR4 is required for outgrowth of colon carcinoma micrometastases. Cancer Res 2003; 63:3833–9.
37. Koshiba T, Hosotani R, Miyamoto Y, et al. Expression of stromal cell-derived factor 1 and CXCR4 ligand receptor system in pancreatic cancer: a possible role for tumor progression. Clin Cancer Res 2000;6:3530–5.
38. Scala S, Ottaiano A, Ascierto PA, et al. Expression of CXCR4 predicts poor prognosis in patients with malignant melanoma. Clin Cancer Res 2005;11: 1835–41.
39. Kim J, Takeuchi H, Lam ST, et al. Chemokine receptor CXCR4 expression in colorectal cancer patients increases the risk for recurrence and for poor survival. J Clin Oncol 2005;23:2744–53.
40. Xu F, Wang F, Di M, et al. Classification based on the combination of molecular and pathologic predictors is superior to molecular classification on prognosis in colorectal carcinoma. Clin Cancer Res 2007;13: 5082–8.
41. Dalerba P, Clarke MF. Cancer stem cells and tumor metastasis: first steps into uncharted territory. Cell Stem Cell 2007;1:241–2.
42. Balkwill F, Mantovani A. Inflammation and cancer: back to Virchow? Lancet 2001;357:539–45.
43. Coussens LM, Werb Z. Inflammatory cells and cancer: think different! J Exp Med 2001;193:F23–6.
44. Burns JM, Summers BC, Wang Y, et al. A novel chemokine receptor for SDF-1 and I-TAC involved in cell survival, cell adhesion, and tumor development. J Exp Med 2006;203:2201–13.
45. Miao Z, Luker KE, Summers BC, et al. CXCR7 (RDC1) promotes breast and lung tumor growth *in vivo* and is expressed on tumor-associated vasculature. Proc Natl Acad Sci U S A 2007;104:15735–40.
46. Wang J, Shiozawa Y, Wang J, et al. The role of CXCR7/RDC1 as a chemokine receptor for CXCL12/SDF-1 in prostate cancer. J Biol Chem 2008;283: 4283–94.
47. Katsumi Y, Kuwahara Y, Tamura S, et al. Trastuzumab activates allogeneic or autologous antibody-dependent cellular cytotoxicity against malignant rhabdoid tumor cells and interleukin-2 augments the cytotoxicity. Clin Cancer Res 2008;14:1192–9.
48. Schatton T, Murphy GF, Frank NY, et al. Identification of cells initiating human melanomas. Nature 2008;451:345–9.

STEM CELLS
TISSUE-SPECIFIC STEM CELLS

Intra-articular Injected Synovial Stem Cells Differentiate into Meniscal Cells Directly and Promote Meniscal Regeneration Without Mobilization to Distant Organs in Rat Massive Meniscal Defect

MASAFUMI HORIE,[a] ICHIRO SEKIYA,[b] TAKESHI MUNETA,[a,c] SHIZUKO ICHINOSE,[d] KENJI MATSUMOTO,[e] HIROHISA SAITO,[e] TAKASHI MURAKAMI,[f] EIJI KOBAYASHI[f]

[a]Section of Orthopedic Surgery, [b]Section of Cartilage Regeneration, Graduate School, [c]Global Center of Excellence Program and International Research Center for Molecular Science in Tooth and Bone Diseases, and [d]Instrumental Analysis Research Center, Tokyo Medical and Dental University, Tokyo, Japan; [e]Department of Allergy and Immunology, National Research Institute for Child Health and Development, Tokyo, Japan; [f]Division of Organ Replacement Research, Center for Molecular Medicine, Jichi Medical University, Tochigi, Japan

Key Words. Mesenchymal stem cells • Synovium • Meniscus • Luciferase • LacZ • Cell transplantation

ABSTRACT

Osteoarthritis in the knees, which can be caused by meniscal defect, constitutes an increasingly common medical problem. Repair for massive meniscal defect remains a challenge owing to a lack of cell kinetics for the menisci precursors in knee joint. The synovium plays pivotal roles during the natural course of meniscal healing and contains mesenchymal stem cells (MSCs) with high chondrogenic potential. Here, we investigated whether intra-articular injected synovium-MSCs enhanced meniscal regeneration in rat massive meniscal defect. To track the injected cells, we developed transgenic rats expressing dual luciferase (Luc) and LacZ. The cells derived from synovium of the rats demonstrated colony-forming ability and multipotentiality, both characteristics of MSCs. Hierarchical clustering analysis revealed that gene expression of meniscal cells was closer to that of synovium-MSCs than to that of bone marrow-MSCs. Two to 8 weeks after five million Luc/LacZ+ synovium-MSCs were injected into massive meniscectomized knee of wild-type rat, macroscopically, the menisci regenerated much better than it did in the control group. After 12 weeks, the regenerated menisci were LacZ positive, produced type 2 collagen, and showed meniscal features by transmission electron microscopy. In in-vivo luminescence analysis, photons increased in the meniscus-resected knee over a 3-day period, then decreased without detection in all other organs. LacZ gene derived from MSCs could not be detected in other organs except in synovium by real-time PCR. Synovium-MSCs injected into the massive meniscectomized knee adhered to the lesion, differentiated into meniscal cells directly, and promoted meniscal regeneration without mobilization to distant organs. STEM CELLS *2009;27:878–887*

Disclosure of potential conflicts of interest is found at the end of this article.

INTRODUCTION

The meniscus is a wedge-shaped semilunar fibrocartilage that lies between the weight bearing joint surfaces of the femur and the tibia. For symptomatic meniscus injury, a meniscectomy is often performed. This, however, often leads to osteoarthritis [1]. Meniscal suture to preserve its function is limited for its indication, and the result is not always satisfactory due to poor healing of the meniscus. Despite other therapeutic attempts [2], problems related to its effectiveness and invasion persist. A novel strategy for meniscus injury remains necessary.

Mesenchymal stem cells (MSCs) are postulated to participate in tissue homoeostasis, remodeling, and repair by ensuring the replacement of mature cells lost to physiological turnover, senescence, injury, or disease. Stem cell populations are found in most adult tissues, and in general, their differentiation potential may reflect the local cell population. Developmentally, intra-articular tissues are differentiated from common progenitors, referred to as common interzone cells [3]. Synovium-MSCs have high

Author contributions: M.H.: conception and design, data analysis, collection of data, and manuscript writing; I.S.: conception and design, financial support, manuscript writing, final approval of manuscript; T. Muneta: conception and design, financial support, and administrative support; S.I.: electron microscopy; K.M.: microarray and real-time PCR; H.S.: microarray and real-time PCR; T. Murakami: provision of study material and manuscript writing; E.K.: conception and design, financial support, administrative support, provision of study material, manuscript writing.

Correspondence: Ichiro Sekiya, M.D., Ph.D., Section of Cartilage Regeneration, Graduate School, Tokyo Medical and Dental University, 1-5-45 Yushima, Bunkyo-Ku, Tokyo 113-8519, Japan. Telephone: +81-3-5803-4675; Fax: +81-3-5803-0266; e-mail: sekiya.orj@tmd.ac.jp; or Eiji Kobayashi, M.D., Ph.D., Division of Organ Replacement Research, Center for Molecular Medicine, Jichi Medical University, 3311-1 Yakushiji, Shimotsuke, Tochigi 329-0498, Japan. Telephone: +81-285-58-7446; Fax: +81-285-44-5365; e-mail: eijikoba@jichi.ac.jp Received July 16, 2008; accepted for publication December 9, 2008; first published online in STEM CELLS *EXPRESS* January 8, 2009. 1066-5099/2009/$30.00/0 doi: 10.1634/stemcells.2008-0616

chondrogenic potential [4, 5], clinically increase in number in synovial fluid after intra-articular tissue injury to contribute to its repair in part [6] and expand in the presence of pure synovial fluid in tissue cultures of the synovium [7]. Synovial tissue may serve as a reservoir of stem cells that mobilize following injury and migrate to the wound site where, in cooperation with local cells, they participate in the repair response.

Thus, during the natural course of meniscal repair, synovium-MSCs are a potential cell source. Here, we investigated whether intra-articular injected synovium-MSCs enhanced meniscal regeneration in rat massive meniscal defect. Dual colored transgenic (Tg) rats expressing luciferase and LacZ (Luc/LacZ) were created for this study so that the fate of transplanted cells could be traced dynamically and precisely.

Materials and Methods

Establishment of Dual Colored Transgenic Rat

Dual colored Tg rats expressing luciferase and Lac-Z were created by cross-breeding ROSA/luciferase Tg Lewis rats [8] with ROSA/LacZ Lewis rats [9]. The expression of luciferase was detected by an in vivo bioimaging system, and the expression of LacZ was detected by X-gal staining (detailed later). The F1 hybrids between ROSA/luciferase Tg and ROSA/LacZ Lewis rat neonate were imaged after *intraperitoneal injection of* D-luciferin (30 mg/kg per body weight) (potassium salt; Biosynth, Postfach, Switzerland, http://www.biosynth.com), and then they were stained with X-gal. In the same manner, luciferase and LacZ expressions were examined in various tissues of these rats. Approximately one-fourth of these F1 hybrids expressed luciferase and LacZ in the whole body. We used these "dual colored" F1 hybrids expressing both luciferase and LacZ (Luc/LacZ) for the donor of MSCs.

MSCs Preparation

All experiments were conducted in accordance with the institutional guidelines for the care and use of experimental animals of Tokyo Medical and Dental University and Jichi Medical University. The synovial membranes of bilateral knee joints were excised, minced, and digested for 3 hours at 37°C with type V collagenase (0.2%; Sigma-Aldrich, St. Louis, MO, http://www.sigmaaldrich.com), and passed through a 40-μm filter (Becton Dickinson, Franklin Lakes, NJ, http://www.bd.com). Bone marrow was extruded by inserting a 22-gauge needle into the shaft of the femur and tibia bone and flushed out. Synovium and bone marrow cells were cultured in a complete medium (αMEM; Invitrogen, Carlsbad, CA, http://www.invitrogen.com; 20% FBS; Invitrogen; 100 units per milliliter penicillin, 100 μg/ml streptomycin, and 2 mM L-glutamine; Invitrogen) for 14 days. Then the cells were replated at 100 cells/cm^2, cultured for 14 days, and frozen at −80°C as passage 1. The stocked cells were rapidly thawed in a water bath at 37°C, plated in a 150 cm^2 dish, and harvested after 5 days. Then the cells were replated at 100 cells/cm^2, cultured for 14 days, and collected for further analyses [5]. For colony-forming assay, 100 cells were plated in 60 cm^2 dishes and cultured for 14 days. The dishes were stained with X-gal, and the same dishes were then stained with 0.5% Crystal Violet.

In Vitro Differentiation Assay

For adipogenesis, the cells were cultured in the adipogenic medium that consisted of a complete medium supplemented with 0.5 μM dexamethasone, 0.5 mM isobutylmethylxanthine, and 50 μM indomethacin. After 4 days, the adipogenic cultures were stained with 0.3% Oil Red-O solution or X-gal solution [10].

For osteogenesis, the cells were cultured in the calcification medium in the presence of 100 nM dexamethasone, 10 mM β-glycerophosphate, and 50 μM ascorbic acid. After an additional 6 weeks, the dishes were stained with 0.5% Alizarin Red solution or X-gal solution.

For in vitro chondrogenesis, 8×10^5 cells were placed in a 15 ml polypropylene tube (BD Falcon, Bedford, MA, http://www.bdbiosciences.com) and pelleted by centrifugation at 450*g* for 10 minutes. The pellets were cultured for 21 days in chondrogenic media, which contained 500 ng/ml BMP-2 (Astellas Pharma Inc., Tokyo, Japan, http://www.astellas.com), in addition to high-glucose Dulbecco's modified Eagle's medium (Invitrogen) supplemented with 10 ng/ml transforming growth factor-β3 (TGF-β3) (R&D Systems Inc., Minneapolis, MN, http://www.rndsystems.com), 10^{-7} M dexamethasone, 50 μg/ml ascorbate-2-phosphate, 40 μg/ml proline, 100 μg/ml pyruvate, and 50 mg/ml ITS+TMPremix (Becton Dickinson). For histological analysis, the pellets were embedded in paraffin, cut into 5-μm sections, and stained with 1% Toluidine Blue [11].

Flow Cytometry

Synovium-MSCs at passage 3 were harvested 14 days after plating. One million cells were suspended in 500 μl phosphate buffered saline (PBS) containing 20 ng/ml fluorescein isothiocyanate (FITC) or phycoerythrin (PE)-coupled antibodies against CD11b, CD45, CD90 (Becton Dickinson), CD34 (Santa Cruz Biotechnology Inc., Santa Cruz, CA, http://www.scbt.com), and CD29 (BioLegend, San Diego, CA, http://www.biolegend.com) As an isotype control, FITC- or PE-coupled nonspecific mouse IgG (Becton Dickinson) was substituted for the primary antibody. After incubation for 30 minutes at 4°C, the cells were washed with PBS and resuspended in 1 ml PBS for analysis. Cell fluorescence was evaluated by flow cytometry in a FACSCalibur instrument (Becton Dickinson); data were analyzed by using CellQuest software (Becton Dickinson).

Oligonucleotide Microarray

For rat meniscal cells, menisci were minced, digested for 3 hours at 37°C with type II collagenase (0.2%; Sigma), and passed through a 40 μm filter (Becton Dickinson). Nucleated cells were plated at 100 cells/cm^2 and cultured in a complete medium. Total RNA was isolated from passage 1 colony-formed cells derived from the synovium, bone marrow [5], and meniscus with the RNeasy Total RNA Mini Kit (Qiagen, Valencia, CA, http://www1.qiagen.com).

A comprehensive microarray analysis was performed using 3 μg of total RNA from each sample and GeneChip Rat 230 2.0 probe arrays (Affymetrix, Santa Clara, CA, http://www.affymetrix.com) [12]. Data analysis was performed with GeneSpring software version 7.2 (Agilent Technologies, Palo Alto, CA, http://www.agilent.com). To normalize the variations in staining intensity among chips, the "Signal" values for all genes on a given chip were divided by the median value for the expression of all genes on the chip. To eliminate genes containing only a background signal, genes were selected only if the raw values of the "Signal" were more than 30, and expression of the gene was judged to be "Present" by the GeneChip Operating Software version 1.4 (Affymetrix). After elimination, expression data of a total of 14,882 probe sets were employed for further analysis. A hierarchical-clustering analysis was performed using a minimum distance value of 0.001, a separation ratio of 0.5, and the standard definition of the correlation distance. A dendrogram was obtained from a hierarchically clustering analysis using average linkage and distance metric equal to one minus the Pearson correlation applied to the microarray data [13].

Meniscectomy and MSCs Injection

Wild-type male Lewis rats at 12 weeks of age (Charles River, Yokohama, Japan, http://www.crj.co.jp) were used (n = 27). Under anesthesia, a straight incision was made on the anterior side of bilateral knee, the anteromedial side of the joint capsule was cut, and the anterior horn of the medial meniscus was dislocated anteriorly with a forceps. The meniscus was then cut vertically at the level of medial collateral ligament, and the anterior half of medial meniscus was excised. The dislocated meniscus was removed and the wound was closed in layers. Immediately after the skin incision was closed, a 27-gauge needle was inserted

at the center of the triangle formed by the medial side of the patellar ligament, the medial femoral condyle, and the medial tibial condyle, toward the intercondylar space of the femur. Then 5 × 10^6 Luc/LacZ$^+$ synovium-MSCs (n = 14) or bone marrow-MSCs (n = 9) in 50 μl PBS were injected into the right knee joint. For the control, the same volume of PBS was injected into the left knee. The rats were allowed to walk freely in the cage.

For control of in vivo Imaging analysis, 5 × 10^6 Luc/LacZ$^+$ synovium-MSCs were injected into the normal right knee of the wild-type Lewis rats (n = 4).

Histology and Detection of LacZ Expression

The whole medial meniscus was collected at 2, 4, 8, and 12 weeks after MSCs injection (n = 3 each time point). The samples were fixed with a fixative solution (0.2% glutaraldehyde, 2 mM $MgCl_2$, and 5 mM EGTA) in PBS for 10-30 minutes at room temperature and washed three times in a washing solution (2 mM $MgCl_2$, 0.01% sodium deoxycholate, and 0.02% Nonidet P40) in PBS. Then they were treated with an X-gal staining solution (1 mg/ml of 5-bromo-4-chloro-3-indolyl-β-D-galactopyranoside, 2 mM $MgCl_2$, and 5 mM potassium hexacyanoferrate [III], 5 mM potassium hexacyanoferrate [II] trihydrate) at 37°C for 3 hours. They were subsequently fixed again in 4% paraformaldehyde and decalcified with 0.5 M EDTA (pH 7.5) for 3 days at 4°C, followed by a gradient replacement with 20% sucrose for 24 hours at 4°C, and then evaluated by Toluidine Blue or Eosin staining of paraffin sections.

Immunostaining

Sections were pretreated with 0.4 mg/ml proteinase K (DAKO, Carpinteria, CA, http://www.dakousa.com) in Tris-HCl for 15 minutes at room temperature for optimal antigen retrieval. Residual enzymatic activity was removed by washes in PBS, and nonspecific staining was blocked with PBS containing 10% normal horse serum for 20 minutes at room temperature. A primary anti-rat monoclonal antibody against human type II collagen (1 : 200 dilution with PBS containing 1% BSA; Daiichi Fine Chemical, Toyama, Japan, http://www.daiichi-fcj.co.jp) was applied to the section which was incubated at room temperature for 1 hour and rinsed again with PBS. Immunostaining was detected by Vectastain ABC reagent (Vector Laboratories, Burlingame, CA; http://www.vectorlabs.com), followed by diaminobenzidine staining.

In Vivo Bioluminescent Imaging

A noninvasive bioimaging system IVIS (Xenogen, Alameda, CA, http://www.caliperls.com) was used for analysis using IGOR (WaveMetrics, Lake Oswego, OR, http://www.wavemetrics.com) and IVIS Living Image (Xenoxgen) software packages [14]. To detect photons from Luc$^+$ cells, undifferentiated MSCs or chondrocyte pellets were suspended in PBS and imaged immediately after the addition of 0.15 mg D-luciferin (potassium salt; Biosynth). Also, for transplanted cell tracking in vivo, D-luciferin was injected into the penile vein of anesthetized rats (30 mg/kg per body weight) under anesthesia with isoflurane. The signal intensity was quantified as photon flux in units of photons per seconds cm^2 per steradian in the region of interest.

Transmission Electron Microscopy

The regenerated tissues at 12 weeks in the synovium-MSCs treated group and control groups were selected and fixed with 2.5% glutaraldehyde in 0.1 M PBS for 5 hours, washed overnight at 4°C in the same buffer, postfixed with 1% OsO_4 buffered with 0.1 M PBS for 2 hours, dehydrated in a graded series of ethanol, and embedded in Epon 812. Ultrathin sections at 90 nm were collected on copper grids, double-stained with uranyl acetate and lead citrate, and then examined with a transmission electron microscope (H-7100, Hitachi, Hitachinaka, Japan, http://www.hitachi.co.jp) [15].

Quantitative Real-Time PCR

Total RNAs were prepared from brain, lung, liver, spleen, kidney, and knee synovium at 3 days after the synovium-MSCs injected rat by RNAqueous Kit (Ambion, *Austin, TX;* http://www.ambion.com) according to the manufacturer's instructions. For the positive control, total RNAs from various organs of Luc/LacZ Tg rat and expanded MSCs including Luc/LacZ positive cell rates ranged from 0.001 to 100% were used. Also total RNAs from various organs of wild-type rat were prepared as a negative control. They were subjected to *real-time PCR* to measure the level of LacZ.

The primer sets for LacZ, (sense, 5′-GGTGCAGAGAGACAGGAACCAC-3′; antisense, 5′-CCTTCATACTGCACAGGTCTGCT-3′) and β-actin (sense, 5′-CCGAGCGTGGCTACAGCTT-3′; antisense, 5′-GGCAGTGGCCATCTCTTGC-3′) were synthesized at FASMAC (Kanagawa, Japan, http://www.fasmac.co.jp).

First-strand cDNA was synthesized using the I Script cDNA synthesis kit (Bio-Rad Laboratories, Hercules, CA, http://www.bio-rad.com) with an Oligo (dT) (12-18mers) primer. Real-time quantitative PCR analyses were performed with the ABI Prism 7700 Sequence Detection System (Applied Biosystems, Foster City, CA, http://www.appliedbiosystems.com) using SYBR Green I PCR reagents (TOYOBO, Osaka, Japan, http://www.toyobo.co.jp/e/) as described previously [12]. To determine the exact copy numbers of the target genes, the quantified concentrations of subcloned PCR fragments of LacZ and β-actin were serially diluted and used as standards in each experiment. Aliquots of cDNA equivalent to 5 ng of total RNA samples were used for each real-time PCR. Data were normalized with β-actin levels in each sample. The copy number is expressed as the number of transcripts per nanogram total RNA.

Statistics

The Mann-Whitney U test was used to compare two groups at each period. p values less than .05 were considered significant.

Results

Synovium-MSCs Expressing Luc/LacZ Genes

The F1 hybrids between ROSA/luciferase Tg and ROSA/LacZ Lewis rat neonate produced luminescence after intraperitoneal injection of D-luciferin (Fig. 1A), and then they were positive for X-gal staining (Fig. 1B). In the same manner, we next examined luciferase and LacZ expression in various tissues of these rats. Approximately one-fourth of these F1 hybrids expressed luciferase and LacZ in whole body including the synovium (Fig. 1C). We termed these "dual colored" rats as Luc/LacZ Tg rats. MSCs were isolated from the synovium of Luc/LacZ Tg rats. In vitro imaging of luciferase activity showed that as few as one thousand MSCs were detected over the background in the linear dose-dependent output of luminescence (Fig. 1D, 1E). Synovium-MSCs from Luc/LacZ Tg rats formed LacZ$^+$ single cell-derived colonies consisting of spindle cells (Fig. 1F). They could differentiate into adipocytes (Fig. 1G) and calcified with LacZ expression in vitro (Fig. 1H). The cells could also form cartilage with expressions of both LacZ and luciferase (Fig. 1I). The cells derived from synovium of Luc/LacZ Tg rat demonstrated characteristics of MSCs, and the dual markers were maintained after the differentiation. Flow cytometric analysis demonstrated that the majority of synovium-MSCs expressed CD29 and CD90, and were negative for CD11b, CD34, and CD45 (Fig. 1J).

Hierarchical clustering analysis revealed that the gene expression of meniscal cells was closer to that of synovium-MSCs than that of bone marrow-MSCs (Fig. 2). This indicates that synovium-MSCs may retain a more advantageous character as a MSC source for meniscal regeneration than bone marrow-MSCs.

Meniscal Regeneration After Intra-articular Injection of Synovium-MSCs

To obtain in vivo evidence to support the synovium-MSCs potential, we performed massive meniscectomy in both sides

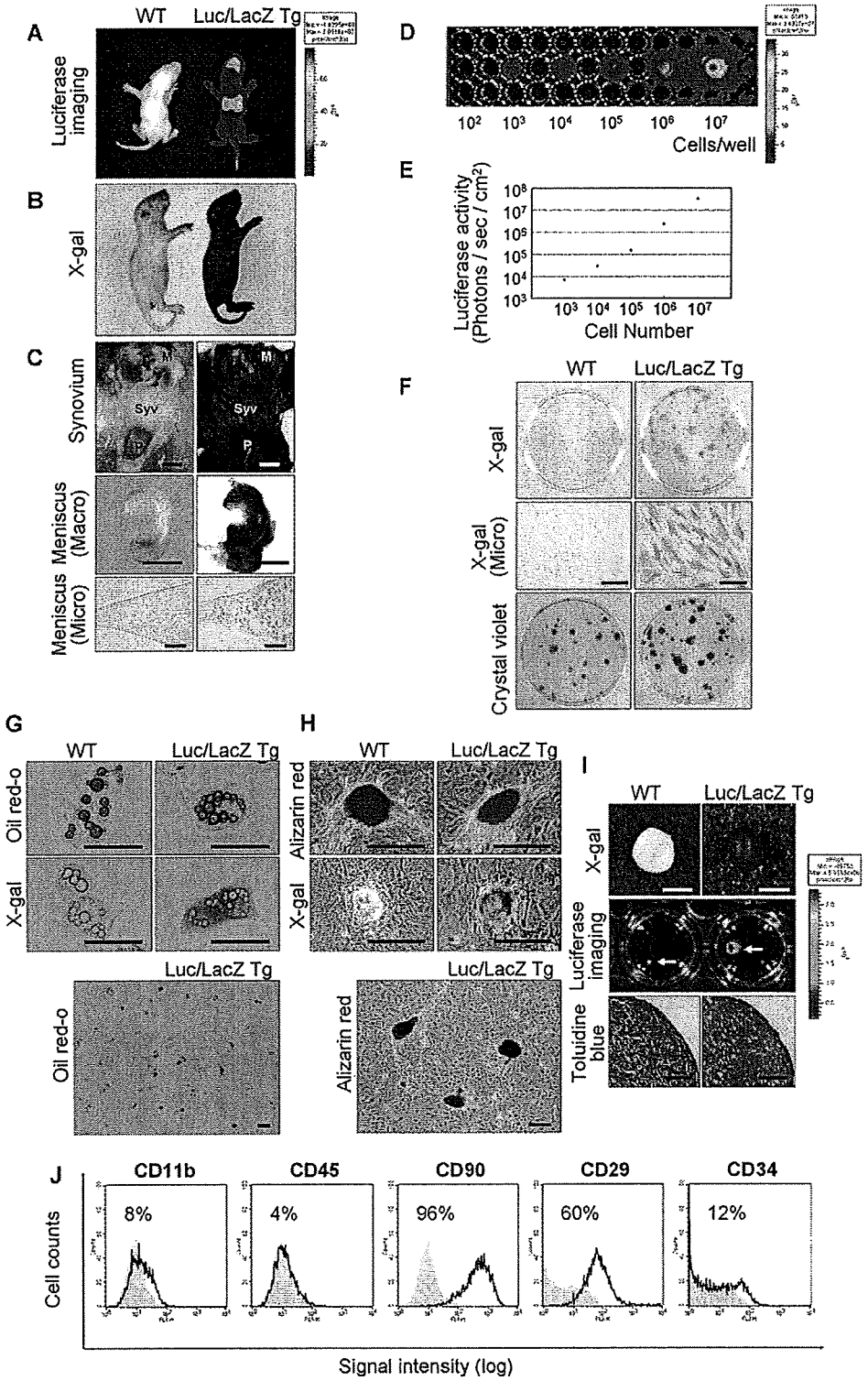

Figure 1. Mesenchymal stem cells (MSCs) derived from the synovium of Luc/LacZ transgenic (Tg) rats expressing dual reporter genes. **(A):** Luminescent images of wild and Luc/LacZ Tg rats. **(B):** Wild and Luc/LacZ Tg rats stained with X-gal. **(C):** Knee synovium and meniscus of wild and Luc/LacZ Tg rats stained with X-gal. Scale bar in upper and middle: 2 mm. Scale bar in lower: 100 μm. **(D):** Bioluminescent imaging of varying numbers of synovium-MSCs from Luc/LacZ Tg rats. **(E):** Quantification for bioluminescent imaging of varying numbers of synovium-MSCs. **(F):** Colony forming ability of MSCs from Luc/LacZ Tg rat synovium. X-gal positive colony forming cells 14 days after the plating of 100 cells in 60 cm^2 dishes (top). Microscopic appearances of X-gal positive spindle cells (middle). Scale bars: 50 μm. Total colonies in the same dishes stained with crystal violet (bottom). **(G):** Adipogenesis. Scale bars: 25 μm. **(H):** Calcification. Scale bars: 100 μm. **(I):** Chondrogenesis. Cartilage pellets stained with X-gal (top). Scale bars: 500 μm. Bioluminescent imaging of cartilage pellets (middle). Histological section stained with toluidine blue (bottom). Scale bar = 100 μm. **(J):** Flow cytometric analysis of synovium-MSCs at passage 3. CD11b, CD45, CD90, CD29, and CD 34 expression are shown as an open plot and isotype control expression as a shaded plot. Abbreviations: M, meniscus; P, patella; Syv, synovium; WT, wild-type.

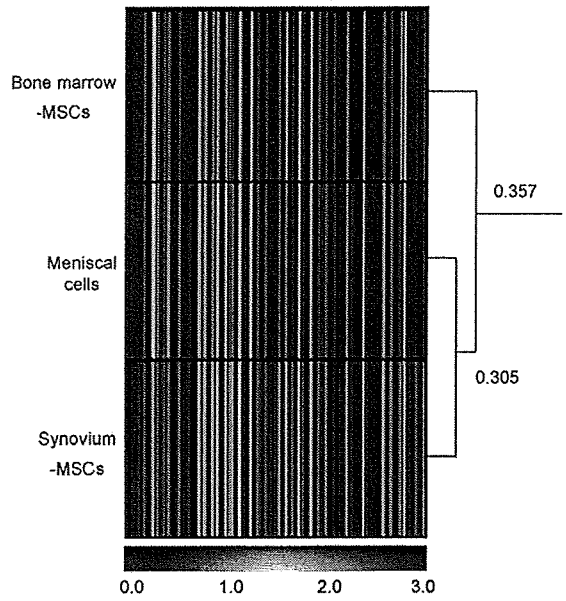

Figure 2. Dendrogram resulting from a hierarchically clustering analysis for gene profile of rat bone marrow-MSCs, synovium-MSCs, and meniscal cells. Gene expression was analyzed with the GeneChip Rat 230 2.0 probe arrays. Data of 14,882 probe sets were analyzed by applying a hierarchical tree algorithm to the normalized intensity. The color code for the signal strength in the classification scheme is shown in the box below. High-expression genes are indicated by shades of red and low expression genes are indicated by shades of blue. The dendrogram at the right provides a measure of the relatedness of gene expression profile in each sample (one minus the Pearson correlation). Abbreviation: MSCs, mesenchymal stem cells.

of the knee of wild rats (Fig. 3A), and Luc/LacZ$^+$ synovium-MSCs suspension (5×10^6 in 50 μl PBS) were injected into the right knee joint immediately after the incision was closed. For the control, the same volume of PBS was injected into the left knee. At 2 weeks, dark blue areas for LacZ were observed around the meniscal defect (Fig. 3B, yellow arrow) and sutured capsule (black arrow), indicating that injected synovium-MSCs intensively adhered to injured sites. Dark blue areas for LacZ were still observed around the meniscal defect and sutured capsule, but not observed in intact synovium, cartilage surface, or cruciate ligaments even at 12 weeks (data not shown). At 4 weeks, the anterior part of the meniscal defect of MSC injection side exhibited better regeneration than the control side (Fig. 3C).

All menisci for the experiment of synovium-MSCs are shown in Figure 3D. At 2 weeks, the regenerated part of the menisci appeared blue after X-gal staining in the MSC injection group, indicating that injected synovium-MSCs contributed to the repair. Square measures of the meniscus in synovium-MSCs injection groups were significantly larger than those in the control groups at 2, 4, and 8 weeks (Fig. 3E). We also evaluated cartilage and observed fibrillation, ones of the degenerative changes on the surface of the medial femoral condyle and medial tibial plateau in the control group at 12 weeks (Fig. 3F).

When we injected the same amount of bone marrow-MSCs, the meniscal defect was more rapidly regenerated than that on the control side at 4 weeks (Fig. 3D). Macroscopically, there were no remarkable differences between the synovium-MSC injection group and the bone marrow-MSC injection group.

Histologically, the contour of the regenerated menisci sharpened and the ultimate forms were closer to the normal meniscal shape (Fig. 4A). Expression of type II collagen increased in a time-dependent manner. LacZ$^+$ MSCs still existed at 12 weeks. In the control group at 12 weeks, regenerated tissue was occupied with less metachromasia, and type II collagen expression was hardly detected. In the bone marrow-MSC injection group, we observed similar features as seen in the synovium-MSC injection group (Fig. 4B).

Electron microscopic analysis of the regenerated meniscus 12 weeks after synovium-MSCs injection demonstrated that round cells with short processes were surrounded by a pericellular matrix, suggesting that meniscal cells were morphologically equivalent to those of the normal meniscus. In contrast, the cell feature in control groups remained to be fibroblastic (Fig. 4C).

Injected MSCs Stay in Knee Joint

The distribution of topically injected synovium-MSCs was evaluated using luciferase-based in vivo imaging. When MSCs were injected into the normal knee ($n = 4$), MSC-derived photons were detected around the right knee, to then decrease within 14 days. When injected into menisectomized knee ($n = 7$), the photons increased in 3 days, then moderately decreased, but could be still observed for 28 days. Substantial luminescence light could not be detected in any other organs of either group (Fig. 5A). Sequential quantification demonstrated that luciferase activities were significantly higher in the meniscectomy group than those in the control group at each time point up to 21 days (Fig. 5B).

To further evaluate whether injected MSCs could migrate to distant organs or not, quantitative real-time PCR was performed. Total RNAs were isolated from the brain, lung, liver, spleen, kidney, and knee synovium of meniscectomized rat at 3 days after the synovium-MSC injection, and were subjected to *real-time PCR* to measure the level of LacZ expression. Injected MSC-derived LacZ gene could be detected only at the injected knee synovium and was not detected in any other organs (Fig. 6). These data confirm the in vivo imaging results and indicate that knee-injected MSCs stayed only in the knee joint.

Discussion

A number of reports have previously described the injection of bone marrow-MSCs into the joint for meniscus injury; however, the kinetics and role of injected MSCs remain unknown. In a goat study, a previously removed medial meniscus regenerated 6 months after MSC injection [16]. However, Caplan et al. suggested in their review article that there were too few prelabeled cells to account for the massive regeneration of the meniscus and inferred that the MSCs trophically enhanced the regeneration of the meniscus [17]. In two other articles, cartilage matrix was present around injected bone marrow MSCs in only a small portion of the injured meniscus, but the roles of injected MSCs were not fully demonstrated [18, 19] To refine our analysis, we created Tg rats expressing dual Luc/LacZ genes.

There are three main factors involved in the interaction between injected synovium-MSCs and meniscal defect: (a) an increase and decrease in the number of the cells, (b) an adherence to the meniscal defect, and (c) differentiation and maintenance.

In in vivo imaging analysis, synovium-MSCs injected into the menisectomized knee transiently increased in number unlike the situation in which the same population of the cells was injected into the intact knee. This indicates that meniscus injury or incision of the articular capsule can produce some cytokines/chemokines to proliferate synovium-MSCs. In a rabbit model,

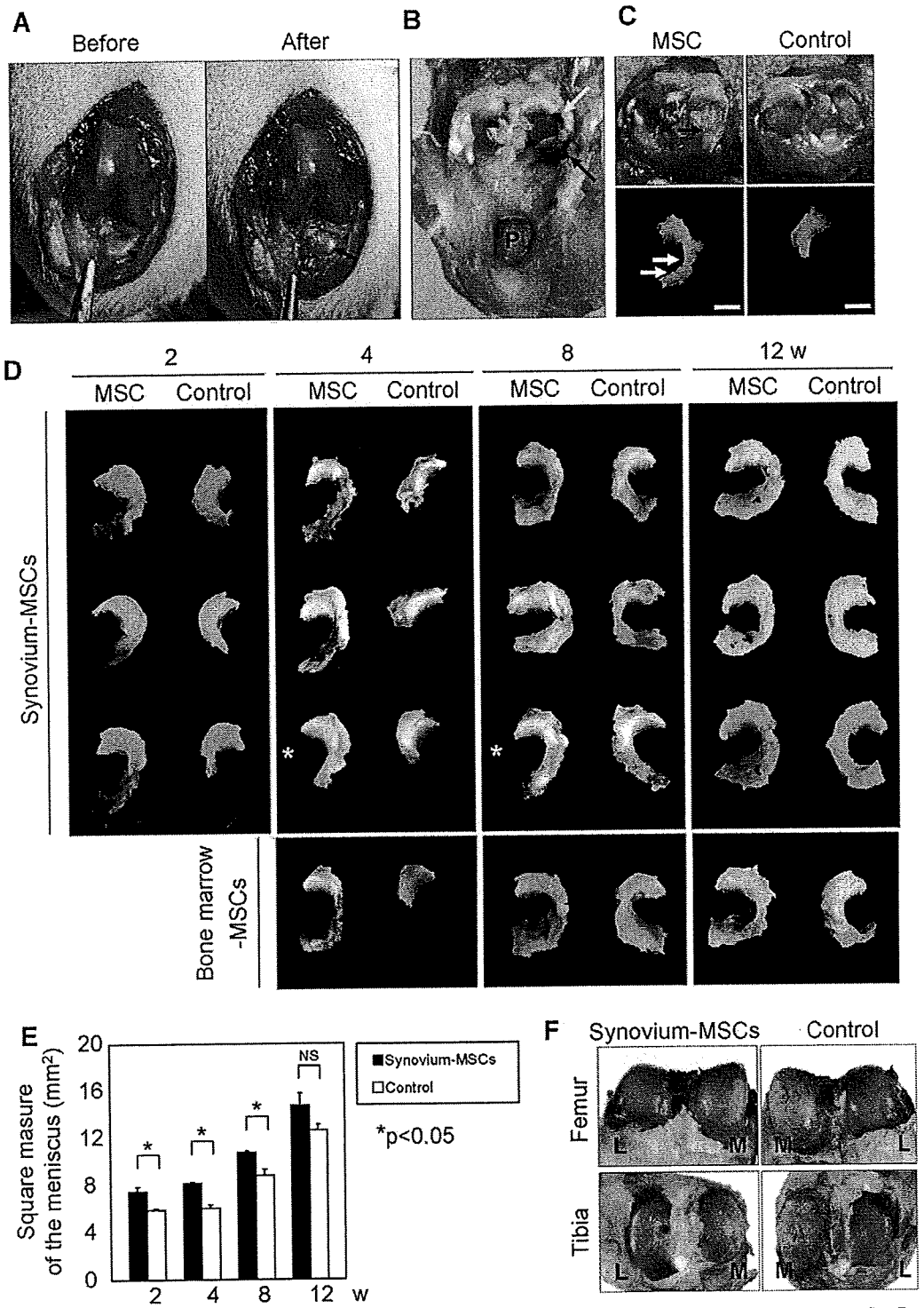

Figure 3. Macroscopic observation of meniscal regeneration after intra-articular injection of synovium-MSCs derived from Luc/LacZ transgenic (Tg) rats. (A): Surgical procedure for massive meniscectomy of a wild rat. The medial meniscus was dislocated anteriorly (left, arrowheads), the anterior half of the meniscus was excised, and tibial cartilage was exposed (right, arrow). (B): Macroscopic findings of the meniscectomized knee 2 weeks after the injection of synovium MSCs. The knee was stained with X-gal. LacZ positive areas were revealed around the meniscal defect (yellow) and sutured capsule (black). (C): Representative macroscopic findings of the tibial joint 4 weeks after synovium-MSCs injection. In the MSC injection group (left), the anterior part of meniscal defect has regenerated (arrow), whereas in the control group, the meniscal defect remains unchanged. Scale bar: 2 mm. (D): Macroscopic findings of the regenerated meniscus at 2, 4, 8, and 12 weeks. All menisci were stained with X-gal except those denoted by an asterisk. Representative macroscopic observation of meniscal regeneration after intra-articular injection of bone marrow-MSCs derived from Luc/LacZ Tg rats are shown in the lower part. (E): Sequential quantification for area of the meniscus. Values are averages with standard deviations ($n = 3$ for each group). *$p < .05$ between the synovium-MSC group and the control group at each period by Mann-Whitney U test. (F): Representative macroscopic findings of the joint surface of femur and tibia 12 weeks after the synovium-MSC group and the control group. The cartilage was stained with India ink. Abbreviations: L, lateral; M, medial; MSCs, mesenchymal stem cells; NS, not significant; P, patella.

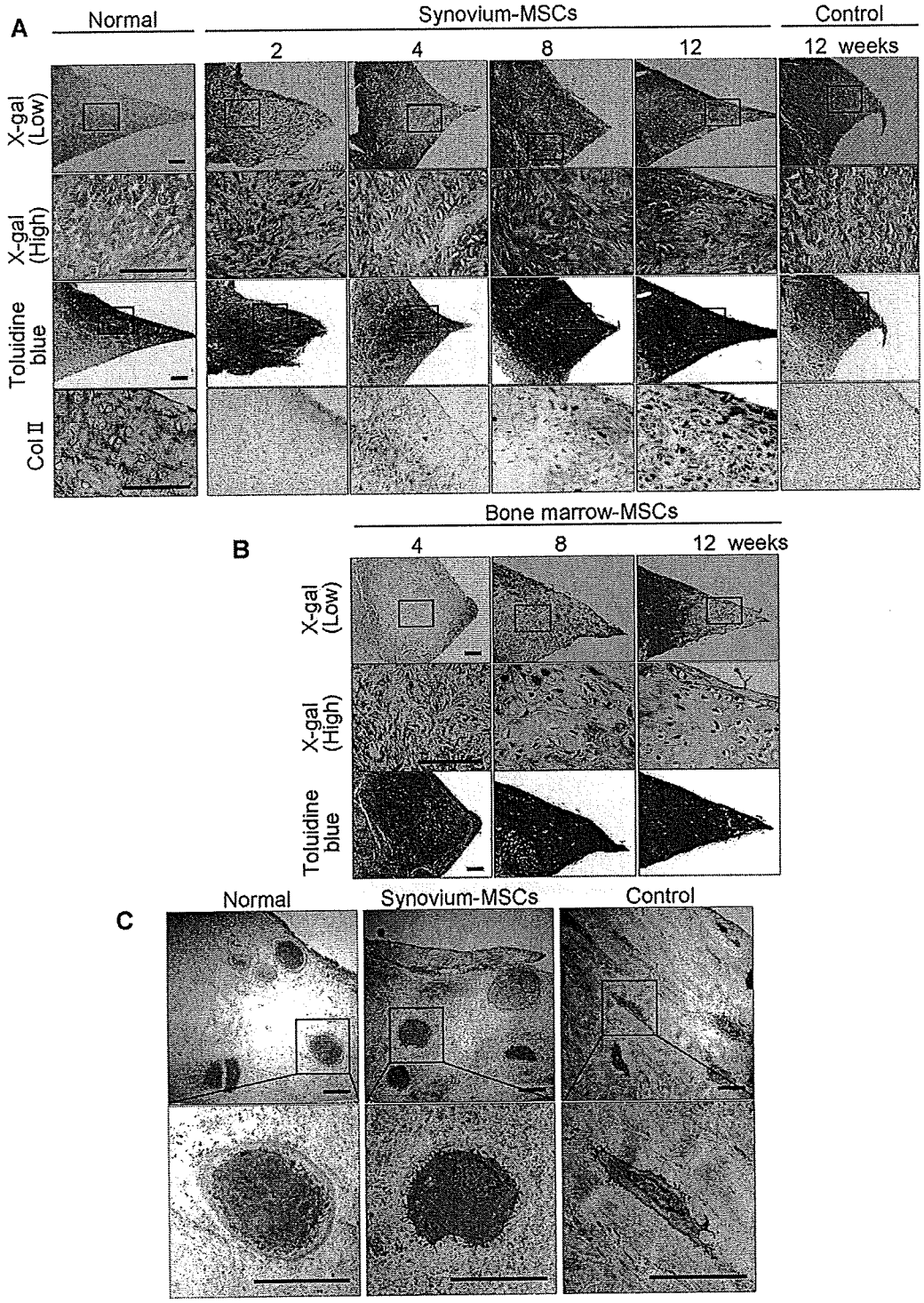

Figure 4. Histological observation of meniscal regeneration after the intra-articular injection of MSCs derived from Luc/LacZ transgenic rats. (A): Representative sections of normal meniscus and regenerated tissues in the synovium-MSC injection group stained with X-gal (and eosin as counter staining), toluidine blue, and immunostained with collagen type 2. Scale bar = 100 μm. (B): Representative sections of regenerated tissues in the bone marrow-MSC injection group stained with X-gal (and eosin as counter staining), toluidine blue. Scale bar: 100 μm. (C): Transmission electron microscopy imaging of typical cells in normal meniscus, regenerated part of meniscus both in the synovium-MSC injection group, and the control group at 12 weeks. Scale bar = 10 μm. Abbreviation: MSCs, mesenchymal stem cells.

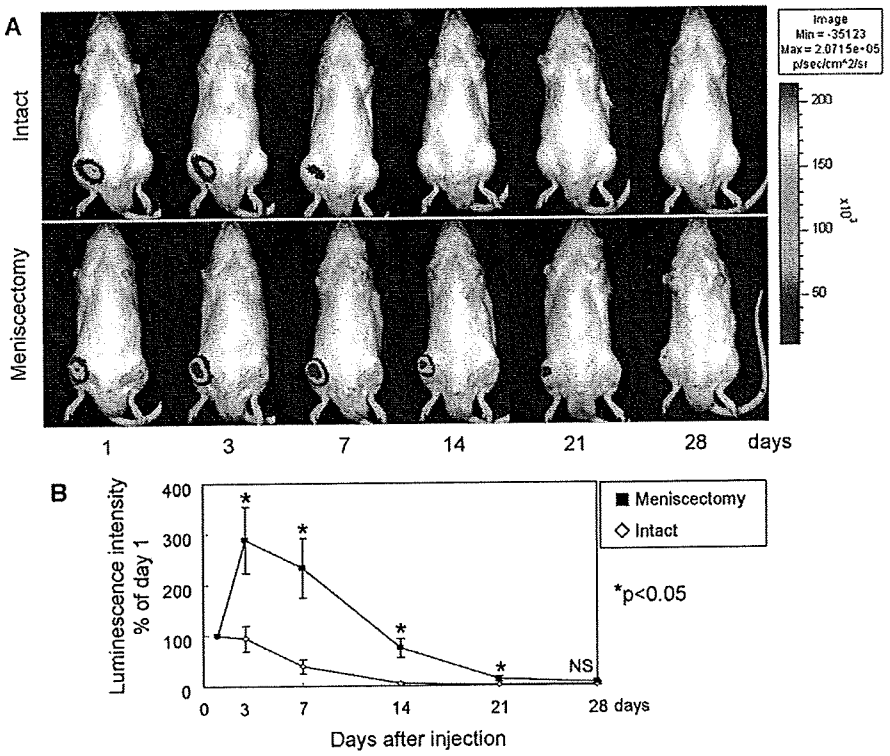

Figure 5. In vivo imaging analysis. (A): Imaging of photons from Luc+ cells. Five million synovium-mesenchymal stem cells (MSCs) derived from Luc/LacZ transgenic rats were injected into the intact knee or the meniscectomized knee. Luciferin was injected into the penile vein at indicated points to monitor luminescence driven by synovium-MSCs. (B): Sequential quantification of luminescence intensity. Average percentages of the value at 1 day are shown with standard deviations. *$p < .05$ between menisectomy group ($n = 7$) and intact group ($n = 4$) at each period by Mann-Whitney U test. Abbreviations: Max, maximum; Min, minimum; NS, not significant.

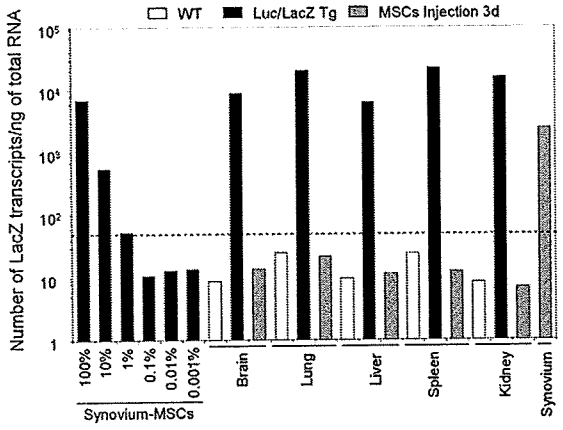

Figure 6. Real-time PCR analysis. The mRNA levels of LacZ obtained from expanded synovium-MSCs and various organs (brain, lung, liver, spleen, kidney, and knee synovium) were determined by SYBR green-based real-time quantitative RT-PCR. The copy number is expressed as the number of transcripts per nanogram of total RNA. The dashed line shows the minimum detection limit (50 copies per nanogram) which was determined by these dilution series. Abbreviations: MSCs, mesenchymal stem cells; Tg, transgenic; WT, wild-type.

meniscal lesions expressed TGF-β, interleukin-1α, and platelet derived growth factor (PDGF) [20]. Human synovium-MSCs have PDGF receptor α and β, and neutralizing PDGF decreases the proliferation of synovium-MSCs in vitro [21]. PDGF may affect the number of transplanted synovium-MSCs.

We could detect MSC-derived photons in the knee joint up to 28 days after the injection but we could not detect it at a longer time point. We have two speculations about this result. One is that a luciferase-based in vivo imaging system cannot detect a small number of Luc^+ cells, as shown in Figure 1D. More than 1,000 cells are needed to detect the light emission. The other is due to blood circulation. The photons are produced only when luciferase is exposed to luciferin substrate and we injected luciferin intravenously. If the Luc^+ cells had existed in the hypovascular area, they could not have been detected. However, in vivo imaging analysis has a great advantage in tracking cells in vivo because we did not have to sacrifice animals, and we could observe the same recipient throughout the observation periods.

Those synovium-MSCs which seem unnecessary for meniscal repair decreased in number and finally fell below measurable limits based on an in vivo imaging system. Possibly, synovium-MSCs participate in intra-articular tissue homoeostasis and repair as do MSCs in mesenchymal tissues throughout the body. This phenomenon differs markedly from ES cells, which form teratomas in the mouse knee joint and subsequently destroy the joint [22]. Induced pluripotent stem cells may hold attraction for future applications, but teratoma formation cannot be overlooked [23].

In vivo imaging analysis suggests that the injected cells did not mobilize out of the injected joint. To confirm this result, we performed real-timePCR to detect Lac Z transcripts. We determined that LacZ transcripts were not detected in brain, lung, liver, spleen, or kidney 3 days after the injection, although the minimum detection limit was 50 copies per nanogram RNA which corresponded to 1% $LacZ^+$ cells. Detection of $LacZ^+$ cells in all sections thorough whole tissues will provide data from another point of view; however, it will be very arduous work.

Injected synovium-MSCs intensively adhered to injured sites of meniscus and synovium. We previously reported that injected synovium-MSCs efficiently adhered to the defect of

articular cartilage [24] and anterior cruciate ligament [6]. The mechanisms that guide the homing of injected cells are not well-understood, but stromal cell-derived factor-1 and monocyte chemotactic protein-1 are candidates to explain them [17].

Undifferentiated synovium-MSCs, attached around the meniscal defect, differentiate into meniscal cells. The environment of the meniscal defect is surrounded by femur and tibia cartilage, synovial tissue, the remaining meniscus, and synovial fluid. The space is also influenced by mechanical stress. This environment itself will provide sufficient signals to induce and maintain meniscal differentiation of synovium-MSCs. Similarly, undifferentiated synovium-MSCs implanted onto an articular cartilage defect differentiate into cartilage cells [25].

In our massive meniscectomized model, bone marrow-MSCs also promoted meniscus regeneration. There were no notable differences of regenerated meniscus in morphology between the synovium-MSC group and the bone marrow-MSC group, although gene profile of synovium-MSCs is closer to that of meniscal cells than that of bone marrow-MSCs. The situation seems to be similar in chondrogenesis as was the case in our previous studies. The gene profile of synovium-MSCs is closer to that of chondrocytes than that of bone marrow-MSCs [26], transplanted bone marrow-MSCs onto the cartilage defect differentiated into chondrocytes at a similar level to that synovium-MSCs which were transplanted in the same way [27]. In contrast, in vivo chondrogenic assay demonstrated that synovium-MSCs produced more cartilage matrix than bone marrow-MSCs [4, 5]. An in vivo model with more sensitivity may distinguish the difference.

Although reparative potential of synovium- and bone marrow-MSCs is similar, synovium-MSCs have an advantage in that they have a higher proliferation potential. In rats, the colony number per nucleated cell was approximately 1/100 in synovium, whereas it was $4/10^5$ in bone marrow. Rat synovium-MSCs expanded much faster than bone marrow-MSCs [5]. Also, human synovium-MSCs proliferated much faster than bone marrow-MSCs when cultured with autologous human serum [21].

For adipogenesis, it usually takes 3 weeks for human bone marrow MSCs to differentiate into adipocytes [10]. In this study, rat bone marrow- and synovium-MSCs differentiated into adipocytes in only 4 days, which was similar to our previous report [5]. Although the content of the adipogenic differentiation medium is similar, the duration to induce sufficient accumulation of lipid vesicles is totally different between MSCs in humans and rats. This indicates the species specificity of MSCs.

For calcification, we found that rat MSCs already calcified in 3 weeks, which was similar to our previous report [5]. In this study, we expected that the calcified area would increase after an additional 3 weeks; therefore, we observed calcification for a total of 6 weeks. Seemingly, the calcified area did not increase during the last 3 weeks (data not shown).

We previously created a 1 mm diameter cylindrical defect in the anterior part of medial meniscus in rats to examine the effect of synovium-MSCs injected intra-articularly. Contrary to our expectation, the cylindrical defect was filled spontaneously, and there was no effect on injected synovium-MSCs through 2-12 weeks [28]. To avoid spontaneous healing, we resected the anterior half of medial meniscus for this study. Meniscal size also increased in the control group, and the difference of meniscal size between the two groups disappeared at 12 weeks; however, the synovium-MSC injected groups showed better results from the standpoint of type II collagen expression and electron microscopic features.

For clinical application, interspecies differences have to be considered. The inherent healing capacity of the meniscus has been shown to be lacking in the inner third and is very limited in the middle third of this poorly vascularized tissue in humans [29] and dogs [30]. We used a rat model, and rat meniscus had a greater spontaneous healing potential. To demonstrate the effectiveness of intra-articular injection of synovium-MSCs for meniscus regeneration, further experimental studies in larger animals are needed.

Native meniscus play an important role in knee stability and shock absorption [31], and this property is linked to the biphasic microstructure of the meniscus [32]. The extracellular matrix of the meniscus is composed mainly of collagen, with smaller quantities of proteoglycans, matrix glycoproteins, and elastin [33]. In this study, we showed that in the synovium-MSC injection group, the menisci regenerated much better than it did in the control group morphologically, and synovium-MSC injection prevented cartilage degeneration at 12 weeks after the meniscectomy as shown in Figure 3F. However, our data lack the details about biomechanical and biochemical properties of regenerated tissues, and it is still uncertain whether the regenerated menisci function in a normal manner and prevent secondary osteoarthritic change in the long term. Therefore, future studies should include biomechanical and biochemical analysis of the regenerated menisci.

Recently, we reported that human synovium-MSCs increased in synovial fluid after intra-articular ligament injury and that exogenous synovium-MSCs adhered to the injured ligament in a rabbit model [6, 34]. We also demonstrated that autologous synovial fluid enhanced migration of MSCs from synovium of osteoarthritis patients in a tissue culture system seemingly to delay the progression of the cartilage degeneration [7]. We speculate that synovial tissue may serve as a reservoir of stem cells that mobilize following intra-articular tissue injury and migrate to the site to participate in the repair response.

According to our speculation, in the case of meniscus injury, MSCs are mobilized from synovium into synovial fluid, and these cells adhere to the injured meniscus. However, the number of MSCs suspended in the synovial fluid and attached to the site is too low to repair or regenerate the injured meniscus, explaining poor spontaneous healing potential of meniscus. Intra-articular injection of synovium-MSCs can boost natural healing ability for meniscal regeneration.

Intravenous infusion of synovium-MSCs may be another route for administration. Although promising results were reported with i.v. infusion of bone marrow-MSCs in animal disease models [35], contrary views are also reported showing that a large fraction of intravenously infused bone marrow-MSCs are trapped in the lung [36]. Cell therapy for meniscal injury has an advantage in that intra-articular injection is possible instead of systemic injection.

The meniscal-deficient knee is a common problem faced by orthopedic surgeons. Although repair of meniscal lesions is possible in selected cases, the poor healing capacity of the tissue often dictates meniscectomy, the most common treatment for meniscal injury. Although meniscectomy provides pain relief and return to function, the loss of meniscal tissue results in long-term dysfunction and secondary osteoarthritis. Currently, there are multiple strategies for addressing this objective, including meniscal allografts, biologic scaffolds for tissue-engineered replacement tissue, and biologic stimuli for meniscal tissue regeneration. In this study, we focused on meniscal regeneration by using synovium-MSCs. Our method has a possibility of regenerating meniscus with less invasion in comparison with meniscal transplantation.

Conclusion

Synovium-MSCs injected into the massive meniscectomized knee adhered to the lesion, differentiated into meniscal cells